Airport Runway Pavement Design for Pre- and Post-COVID-19 Air Traffic

By: Emily Bowler

Advisor: Professor Rajib Mallick

Major Qualifying Project 2020 – 2021

Abstract

The COVID-19 pandemic has brought significant changes to the airline industry. The type and number of aircrafts being operated have changed. The objective of this Major Qualifying Report (MQP) was to evaluate the impact of these changes on the design lives of a runway pavement. Four different scenarios have been analyzed, and the total cost of the designed pavement has been determined. The four scenarios include: pre-COVID-19 air traffic, reduced passenger and increased freight traffic, pre-COVID-19 and expected supersonic traffic, and a combination of reduced passenger, increased freight, and expected supersonic air traffic. Mechanistic-empirical designs were conducted with the help of layered elastic analyses of stresses and strains as well as with transfer functions from the Federal Aviation Administration (FAA) airport pavement design process. Cumulative damage factors (CDF) for each aircraft, and the effect of the different scenarios on them have been presented.

Table of Contents

Contents

Acknowledgements

I would like to acknowledge the help of Ms. Sarah Dennechuk, a Senior Project Manager for the Massachusetts Port Authority for providing information on Logan International Airport's air traffic and the details of a runway pavement structure.

Table of Figures

Table of Tables

0.1 Proposal

The goal of this project was to develop and compare designs of airport pavements with considerations of existing and future air traffic. To achieve this project goal, multiple steps were followed. The main steps to reach the goal have been outlined in *Figure 0-1: Project Process*.

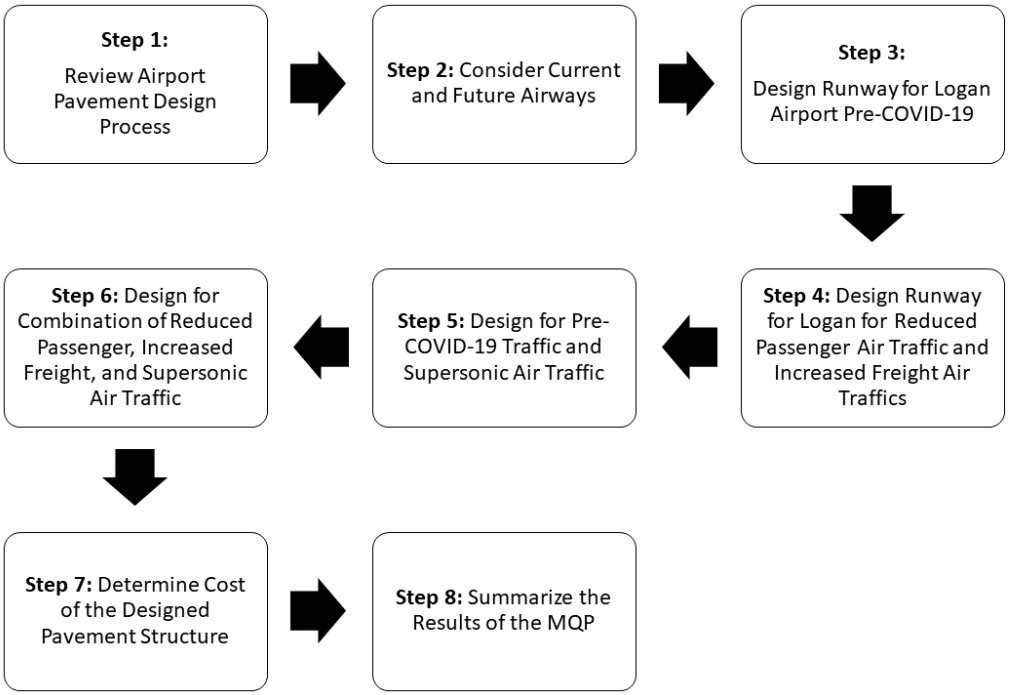

Figure 0-1: Project Process

Steps One (Review Airport Design Process) and Two (Consider Current and Future Airways), were research-based steps. These two main steps provided the basic information and guidelines for the rest of the project. The two differ in that Step One (Review Airport Design Process) was the method of designing an airport pavement structure and Step Two (Consider Current and Future Airways) consisted of information on the changes in air traffic that was implemented in the rest of the project's designs. These changes consisted of adding or altering aircraft types and changing the number of departures.

Step Three (Design Runway for Logan Airport Pre-COVID-19) was the 'control' design of this report. In this chapter, a runway pavement for the Logan International Airport (Boston) was designed with the current (pre-COVID, from 2019) Logan Airport traffic data for a design life of ten years. Only the expected traffic growth was considered for this design.

Steps Four (Design Runway for Logan for Reduced Passenger Air Traffic and Increased Freight Air Traffics) and Five (Design for Pre-COVID-19 Traffic and Supersonic Traffic) were the resulting combination of Steps One (Review Airport Design Process) and Two (Consider Current and Future Airways). In Step Four (Design Runway for Logan for Reduced Passenger Air Traffic and Increased Freight Air Traffics), a design was developed from the Logan Airport pavement with considerations to varying quantities of freight aircrafts and smaller aircrafts. Step

Five (Design for Pre-COVID-19 Traffic and Supersonic Traffic) focused only on the impact of additional expected commercial supersonic aircrafts on pavement.

Step Six (Design for Combination of Reduced Passenger, Increased Freight, and Supersonic Traffic) combined all design alterations from previous steps into one design (i.e., decreased passenger, increased freight, and expected supersonic air traffic).

In Step Seven (Design Cost of the Designed Pavement Structure), the cost of the design was estimated. Along with cost estimation, the different resulting CDF values were compared. The CDFs form the basis of pavement structure analysis and design.

In Step Eight (Summarize the Results of the MQP), the results from the MQP were summarized.

0.2 Introduction

The goal of this project was to develop and compare designs of airport pavements with considerations for existing and future air traffic. The steps – as previously stated in the proposal section– to complete this project can be grouped as seen in *Figure 0-2: Project Steps.* The first group of steps necessary to complete this project was to review content related to pavement design and air traffic changes. The next group of steps were implementing the material from the first group into designing a pavement with no alterations and various pavement designs with some form of an alteration that reflect the expected changes in air traffic. The last group of steps would be to compare the designs based on CDFs and cost. These comparisons could be used for the recommendation of an appropriate design.

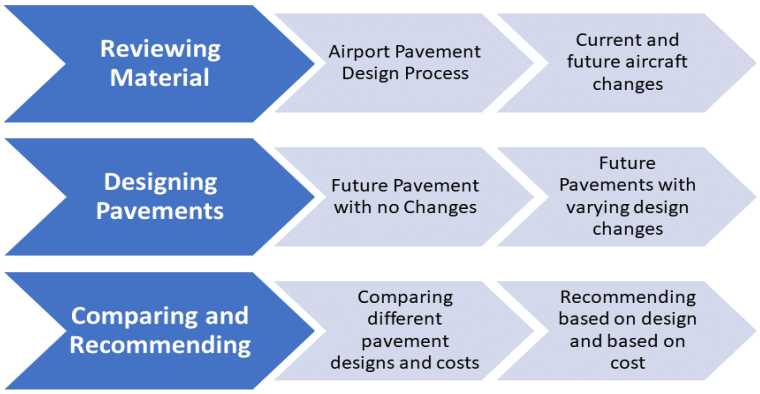

Figure 0-2: Project Steps

The main problem to focus on for the designs will be what factors will be causing damage or failure. Progressive damage and eventual failure of a pavement is caused by either structural rutting or bottom-up fatigue cracking. Within the design process, the rutting and cracking failure potentials of the pavement are evaluated (Mallick & El-Korchi, 2017). Cracking can be caused by multiple issues. The main form of cracking is due to fatigue failure, caused by the "repeated [creation of] tensile stresses/strains at the bottom of the asphalt mix layer…" (Mallick & El-Korchi, 2017). Structural rutting is caused by the repeated appearance of compressive stresses/strains on top of the soil subgrade (Mallick & El-Korchi, 2017). In addition to the consideration of the pavement structure, the expected changes in air traffic were also taken into account when designing an airport pavement structure for a certain design life, and these changes were discussed in *Chapter Two: Current and Future of Airways.*

Measures can be taken to prevent the calculated damages. In the case of rutting or cracking failure, steps within the immediate design process can be considered (Mallick & El-Korchi, 2017). As for the current and future changes, multiple designs and a final recommended design will be presented in this MQP. Note that because the design involved an existing runway pavement (Runway 9/27), only the thickness of the surface layer was altered during the design process.

1.0 Review of the Airport Pavement Design Process

An overview of the airport pavement design process is shown in *Figure 1-1: Airport Pavement Design Process* (Mallick & El-Korchi, 2017; United States Department of Transportation: Federal Aviation Administration [USDOT: FAA], 2016a). The following figure's process has been formalized in the software FAARFIELD (United States Department of Transportation: Federal Aviation Administration [USDOT: FAA], 2016b). For this MQP, the pavement design process utilized a combination of spreadsheets and layered-elastic analysis design software, rather than using FAARFIELD (USDOT: FAA, 2016b). The spreadsheet approach enabled the designer to use specific equations as needed, as well as estimate, visualize and compare the damages caused by the different aircrafts.

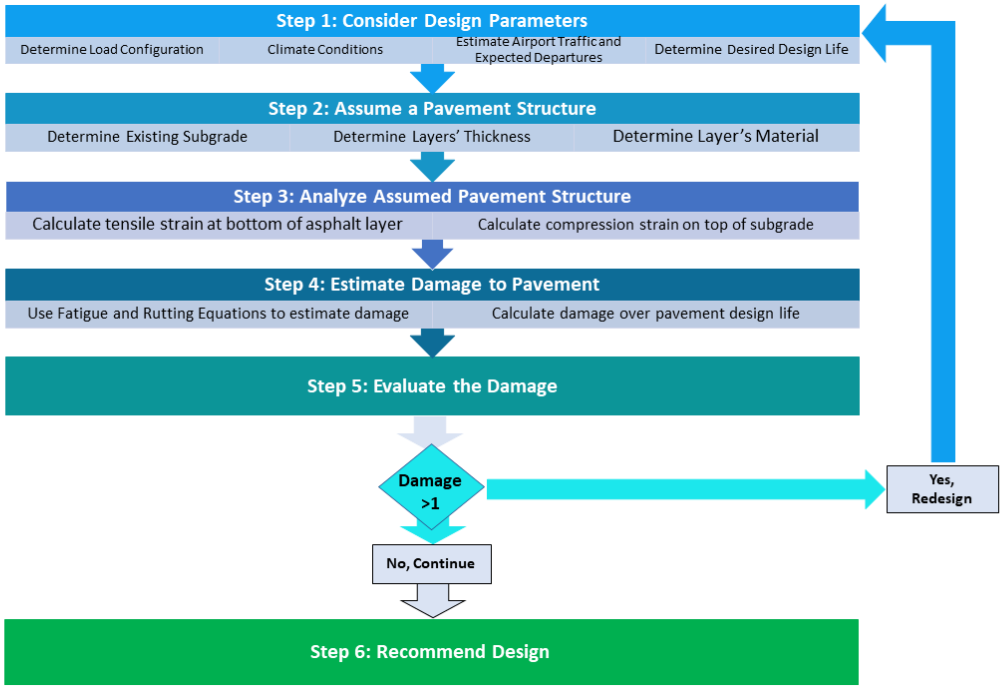

Figure 1-1: Airport Pavement Design Process (Mallick & El-Korchi, 2017; USDOT: FAA, 2016a)

In step one, the design parameters need to be considered prior to evaluating a pavement design option because the stated factors – climate, design life, departure/air traffic, and load configuration – impact the decision for the pavement layers (Mallick & El-Korchi, 2017; USDOT: FAA, 2016a). The first part of step 1 is to determine the aircrafts that use the airport runway, their gross loads, wheel numbers and spacing. This allows for the determination of the maximum expected load and the surface area in contact through which the loads are applied (Mallick & El-Korchi, 2017). Estimation of the departure traffic, aircraft loads, and the expected growth factor are needed (Mallick & El-Korchi, 2017). At this point, the design life of the pavement needs to be decided because this determines how long the pavement's structure will perform adequately before failure (by either cracking or rutting) from repeated load impact, and when rehabilitation becomes necessary (Mallick & El-Korchi, 2017; USDOT: FAA, 2016a). The last aspect of step one is to consider the climate conditions of the project location. This is due to the environment impacting both the

materials of the pavement layers and the soil of the subgrade (Mallick & El-Korchi, 2017; USDOT: FAA, 2016a). Temperature and moisture are the key environmental related conditions that impact the soil subgrade and the upper layers of airport pavements (Mallick & El-Korchi, 2017; USDOT: FAA, 2016a).

Step two of the process considers the factors determined in step one and applies the knowledge in deciding the layers and materials of the pavement structure. The typical pavement structure for airport pavements consists of (starting from the bottom) the subgrade, subbase, base, and surface layer (USDOT: FAA, 2016a). Each layer must meet the materials and minimum thickness criteria that have been mandated by the FAA (FAA, 2016a). The elastic modulus, Poisson's ratio and slip condition (between two successive layer) are needed for the layered elastic analysis (LEA) analysis that was conducted with the WinJULEA software (Engineering Research & Development Center [ERDC–WES], n.d.).

In step three, a LEA is conducted to determine stresses and strains at critical locations, generally with the help of a software, such as WinJULEA (ERDC-WES, n.d.). From the values determined in steps one and two – layer thickness, layer material, aircraft tire contact area, tire spacing, elastic modulus, and Poisson's Ratio – the software, WinJULEA, calculates the tensile and compressive strains in the different layers (ERDC – WES, n.d.). Below, *Figure 1-2: WinJULEA Calculation Process*, explains the steps to use the WinJULEA software. To use this software each entry box needs to reflect the order of the pavement layers from top to bottom – surface to subgrade. Once these values are input into the designated boxes and 'calculate' is selected, the compressive and tensile strain, at the critical locations (which had been specified)– along with other calculations – are output which then can be utilized for step four (ERDC – WES, n.d.).

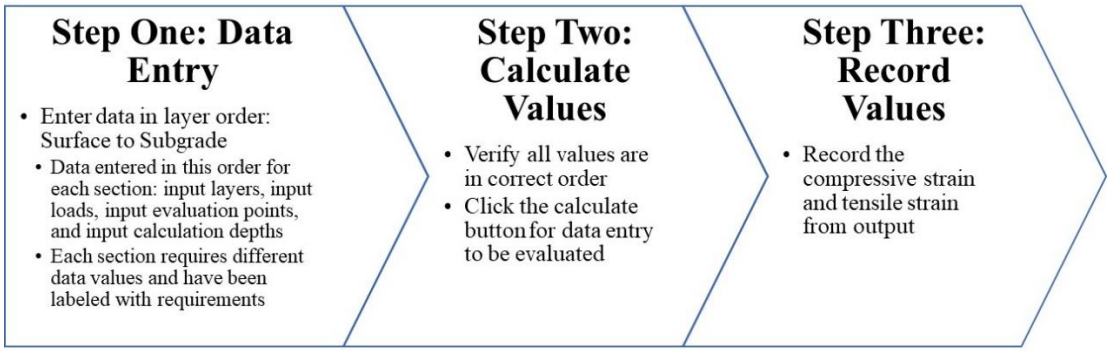

Figure 1-2: WinJULEA Calculation Process (ERDC-WES, n.d.)

Step four takes the values calculated from the earlier steps and applies them into two equations, the fatigue cracking equation and rutting equation, which calculate the numbers of repetitions to failure in the pavement layers (Mallick & El-Korchi, 2017). Equation 1-1 shows the rutting equations and Equation 1-2 shows the fatigue cracking equation (Mallick & El-Korchi, 2017).

$$C = \left(\frac{0.004141}{\varepsilon_v}\right)^{8.1}$$ ----------(1-1a)

For C<1,000 passes

$$\log_{10}(C) = \left(\frac{1}{-0.1638+185.19\varepsilon_v}\right)^{0.60586}$$ ----------(1-1b)

For C > 1,000 passes

Where:

ε_v = compressive strain on top of the subgrade fromLEA

For this MQP, only Equation 1-1a was used.

$$N_f = 0.4801PV^{-0.9007}$$ ----------(1-2)

Where:

$$PV = 44.422\varepsilon_h^{5.140}S^{2.993}VP^{1.850}GP^{-0.4063}$$

ε_h = tensile strain at the bottom of the asphalt mix layer from LEA

S=600,000 psi

V_a= 3.5%

V_b=12%

PNMS = 95%

PPCS=58 %

P200 = 4.5 %

$VP = V_a/(V_a + V_b)$

$GP = (PNMS - PPCS)/(P200)$

Once the equations have been solved with the previously found values, the number of actual repetitions are divided by the allowable repetitions for rutting (C) and fatigue (N_f) separately, to determine the corresponding rutting and fatigue damage (two separate damage factors). The one with the lower allowable repetitions (and hence the higher ratio) becomes the critical damage factor/dominant failure mechanism (Mallick & El-Korchi, 2017). Equation 1-3 shows the generic equation to calculate the expected damage and Equation 1-4 is cumulative form (Mallick & El-Korchi, 2017).

$$Damage = \frac{n}{N}$$ ----------(1-3)

$$Cumulative\ Damage = \sum_{i=1}^{n}\frac{n_i}{N_i}$$ ----------(1-4)

Where:

n = calculated total load

N = allowable repetitions to failure

i = 1-n, represents the different types of aircrafts

In step five the cumulative damage calculated in step four for rutting and fatigue are each checked against a value of 1. If the CDF value exceeds 1, then the pavement is under-designed, and the design process must be repeated. This is due to the design reaching the end of its design life sooner than the planned design life (Mallick & El-Korchi, 2017). This indicates a re-design through a selection of better materials and/or thicker layers. If the CDF value is less than 1, the process can continue onto step six as there is no issue with the

assumed design (Mallick & El-Korchi, 2017). However, if the value is significantly less than 1, then the pavement is overdesigned, and a redesign would be required to avoid an unnecessary thick and costly structure (Mallick & El-Korchi, 2017).

In step six, the most appropriate design is selected from the above steps and recommended for construction.

2.0. Current and Future of Airways

This chapter discusses the changes to air traffic caused by the COVID-19 pandemic.

2.1. COVID-19

COVID-19 has caused profound changes to aircrafts and air travel. COVID-19 was a new coronavirus disease that broke out in 2019 (Centers for Disease Control and Prevention [CDC], 2020). Prior to being declared a pandemic and as information about the disease was being shared, basic steps to prevent the spread of COVID-19 were announced and began being implemented in some places (World Health Organization [WHO], 2020). After the disease was declared a pandemic, preventative measures increased (WHO, 2020). A resulting preventative measure was countries locking down and thereby cutting travel or stopping it entirely (Suau-Sanchez et al., 2020).

There was an immediate impact to air travel, and studies had been conducted to predict the expected and resulting impact of COVID-19 on air travel (Iacus et al., 2020; Suau-Sanchez et al., 2020). These studies were considering the bounce back of passengers returning to travel and the impact it has for airlines/air travel as well as the overall economic impact (Iacus et al., 2020; Suau-Sanchez et al., 2020). Other relevant factors that have impacted travel include the social distancing safety guidelines that have been implemented in airports and some aircrafts (Walton, 2020).

Overall, there is a significant amount of uncertainty regarding the future of air travel and the airlines industry.

2.2. Increase in the Use of Smaller Aircrafts

Prior to COVID-19, increasing the range of relatively smaller size aircrafts and introducing bigger aircrafts was a planned change for air travel. To provide a specific example, Airbus had announced intentions to modify existing and/or to add new models of single-aisle aircrafts that would travel longer distances (Josephs, 2019). Changes to the smaller aircrafts were being made to provide improvements. To look at a specific example of an Airbus aircraft, the A350-900 has both its standard A350-900 version and a long-distance version – A350-900ULR – that modified aspects of the initial design to allow for travelling further distances (Airbus, n.d.).

Airbus is not the only company adapting their smaller models. Since as early as 2004, the Boeing 777 series has made continual improvements in the overall design, materials used, engine efficiency (both for power and fuel used), environmental impact, and increased traveling distance – to name a few features – to provide an aircraft that would be more attractive to the aviation industry (Boeing, n.d.)

2.3. Modifying Passenger Aircrafts to Freight Aircrafts

Another planned change to airlines was an increase in freight aircrafts. This change was seen by Boeing who – when planning for the next 20 years – saw a need for more freight aircrafts (“Proactive Investors: Boeing ups its 20-year industry forecast for passenger and freight planes demand by 4”, 2017). Both Boeing and Airbus provide freight aircrafts with varying volume and load capacities with different origins (Cummins, 2020). These origins range from designing new freight aircrafts to modifying aircrafts previously used as passenger aircrafts (Cummins, 2020). A study by Nahum et al. (2019) concluded that using a combination of cargo specific aircrafts and passenger

aircrafts as partial cargo aircrafts provided the most optimum method of cargo transportation. The use of passenger aircrafts as freight aircrafts also became a trend during the start of the COVID-19 pandemic (Smith, 2020). Airlines switched to freight as a result of COVID-19 to remain economically viable under significantly decreasing passenger revenue (Smith, 2020). Some examples of airlines that have adapted passenger aircrafts for cargo transport are American Airlines Group Inc., Asiana Airlines, Finnair, and Azul Airlines (Kulisch, 2020; Smith, 2020). Both out of pressure from COVID-19 and prior potential, passenger aircrafts are being increasingly used as freight aircrafts. One latest use of passenger aircrafts for freight transport is that by Emirates SkyCargo to ferry COVID-19 vaccines to the different parts of the world (Emirates, n.d.).

2.4. Commercial Supersonic Aircrafts

Commercial supersonic aircrafts are returning. They were brought into operation in the 1970's; however, their use ended in the early 2000's due to both environmental concerns and safety conditions (Boyd, 2019; Turner, 2020; United States Department of Transportation: Federal Aviation Administration [USDOT: FAA], 2020). Recently the FAA has been modifying their rules regarding supersonic aircraft noise and certification process to allow for more advancement in this technology (USDOT: FAA, 2020). While the rules are being modified so are the designs for the aircraft itself. For example, Boom Supersonic (2019, 2020) has noted changes to the supersonic aircrafts that consists of significant improvements in the overall design, engine, fuel, and exterior material. The environmental changes are especially important as both the amount of greenhouse gas and noise levels caused by the aircraft's speed cause great concern (Turner, 2020). With a combination of significant design changes and regulations, it seems that supersonic aircrafts will be returning to the skies in the near future (Boyd, 2019).

2.5. Aircraft Images

Figure 2-1 through 2-6 show the more important (in terms of gross weight) aircrafts that have been considered in this study.

Figure 2-1: A350-900 (Icarus, 2020)

Figure 2-2: Boeing 777 (Abbot, 2014)

Figure 2-3: Freight Aircraft DC-10 (Oertle, 2014a)

Figure 2-4: Freight Aircraft, B747 (Oertle, 2014b)

Figure 2-5: Conceptual Boom Supersonic Aircraft (Boom Supersonic, n.d.)

Figure 2-6: Airbus A380 (Lappin, 2007)

3.0 Design of Runway for Boston Logan International Airport with Existing Air Traffic

The purpose of this chapter was to design a runway for the pre-COVID-19 air traffic (control design). This design will act as a control due to no alterations – beyond a yearly two percent (2%) growth – to the aircraft data. The air traffic data consists of departures from Boston Logan International Airport for the entirety of 2019 (S. Dennechuk, personal communication, October 7, 2020). After a consideration of the rapid changes in the aviation industry, a decision was taken to use 10 years as the design life of the pavements.

This chapter is both an application of the steps outlined in *Chapter 1: Review Airport Design Process*, and additional data research/interpretation of the Boston Logan International Airport aircraft data log. The interpretation of the aircraft logs will occur to some extent for each design chapter; however, this initial design interpretation will be the base for all other versions.

Boston Logan International Airport, shown in *Figure 3-1*, is in Boston, Massachusetts, (42° 22’ 1.1208” N: 71° 1’ 20.5032” W) a city in the United States (Boston Logan Airport, n.d.; Logan International Airport (BOS), Boston, MA, USA, n.d.). Depending on the month the average temperatures vary – to show how much of a contrast it is, the lowest average temperature is 23 degrees Fahrenheit in January and the highest average temperature is 81 degrees Fahrenheit in July (Climate – Boston (Massachusetts), n.d.). Similarly, the amount of precipitation and what form it comes down in varies depending on the month/season but regardless of its form, the average amount of precipitation per month ranges from 3.3 to 4.3 inches (Climate – Boston (Massachusetts), n.d.).

Figure 3-1: Boston Logan International Airport (Google, n.d.)

3.1. Logan International Airport Data

The Logan International Airport air traffic data (*Figure A-1* in the appendix) was considered to identify all aircraft types departing in 2019. In total 212,102 individual aircrafts departed from Logan International Airport in 2019. These 212,102 different aircrafts are made up of 240 aircraft types identified from the data. Within these 240 aircraft types, there exist an 'UNKN' and an 'XXXX' type which are unidentified aircraft types. The combined percentage the unidentified aircrafts account for in the data is 0.0669%. These aircraft types were not used in the design. As a result, the aircraft types have now been adjusted to 238 types with a total of 211,960 individual aircrafts in 2019. To each aircraft types listed in 2019, a 2% growth was applied to their quantity for each year for the next ten years – until the year 2029. The cumulative number of aircrafts taking off in the next ten years was 258, 378 aircrafts. The identified aircrafts were then searched in FAARFIELD to determine the gross weight, number of wheels, wheel spacings, and tire pressures (USDOT: FAA, 2016b).

For the design process, from the list of aircrafts that were found in FAARFIELD the ten aircraft types with the heaviest gross taxi weight were used. The aircrafts are as follows: A343, A345, A346, A359, A388, B744, B748, B74S, B77L, and B77W (USDOT: FAA, 2016b). These aircrafts accounted for 13.0% of the total number of aircrafts that are expected to takeoff from Logan International Airport. Considering the fact that there are six runways, only a third of this air traffic was considered for design of a specific runway. As a result, the total number of aircrafts used was 11,202 which accounts for 4.33% of the total.

3.2. Runway Pavement Structure

The different layers of Runway 9/27 at Logan Airport are as follows: 5 inch of FAA P-401 asphalt, 9 inch of FAA P-401 asphalt base, 9 inch of P-209 crushed aggregate base course, and 16 inch of P-154 subbase (S. Dennechuk, personal communication, October 30, 2020).

Table 3-1 provides the necessary values associated with the layers and materials that were used to calculate the strains at the critical locations from the LEA.

Table 3-1: Pavement Layer Data (USDOT: FAA, 2016a)

Order	Layer	Elastic Modulus (psi)	Poisson's Ratio	Slip
Surface	P-401 Surface	200,000	0.35	0
Base	P-401 Base	400,000	0.35	0
Aggregate	P-209 Crushed Aggregate	75,000	0.35	0
Subbase	P-154 Subbase	40,000	0.35	0
Subgrade	N/A	15,000	0.35	0

3.3. Logan International Airport Pavement Design for 2029

After having identified both the design parameters and the pavement structure, calculations for the design can proceed. To complete *Step 3: Analyze Assumed Pavement Structure*, use of the software WinJULEA is required (ERDC – WES, n.d.).

Figure 3-2 is an example of the WinJULEA screen output with information for the A343 aircraft for Design 1. In *Figure 3-2, the* details for the A343 aircraft and pavement Design 1 are visible on the left half. On the right the computed stresses and strains for the pavement layers are visible. In this step the pavement layers, their properties, loads, contact areas, and critical locations for the computation of strains were input. The load and the contact area for each wheel was calculated as follows:

Load Calculations (Mallick & El-Korchi, 2017)

Load carried by main gear = 95% of gross weight

Load carried by each wheel = Load carried by main gear/ total number of wheels

Contact Area = Load carried by each wheel/tire Pressure

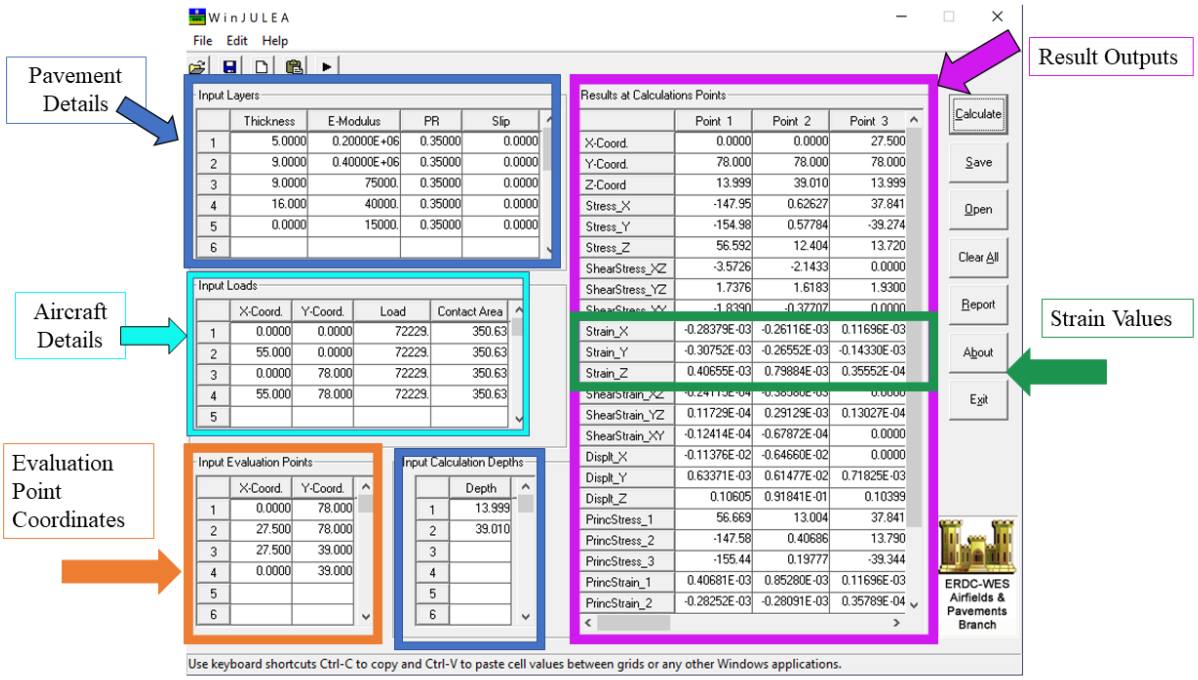

Figure 3-2: Screenshot of WinJULEA used for LEA

While each aircraft's information was processed in WinJULEA, the highest radial tensile strain (Strain X or Strain Y) at the bottom of the lowermost asphalt mix layer, and the vertical compressive strain (Strain Z) on top of the subgrade were recorded for each aircraft. These strains were then utilized in the corresponding rutting or fatigue cracking equation. It is important to note that for the fatigue cracking equation the default/assumed values were used (Mallick & El-Korchi, 2017; Shen & Carpenter, 2007). After the value was found the damage from a single pass of that specific aircraft type was calculated and recorded. Then the CDF for rutting and fatigue were estimated. The CDF values from all

aircrafts were then further combined to get the overall respective CDF for the design. Each of the two overall CDF values (rutting and fatigue) are then compared against 1 to determine if the design is over or under designed. *Figure 3-3*, *Figure 3-4*, and *Figure 3-5* were taken from Design 1 of Aircraft A343 to illustrate the overall process as it went through the spreadsheet. Note, not everything included on the spreadsheet pages are visible in the figures, and that there may be an overlap of material for clarity.

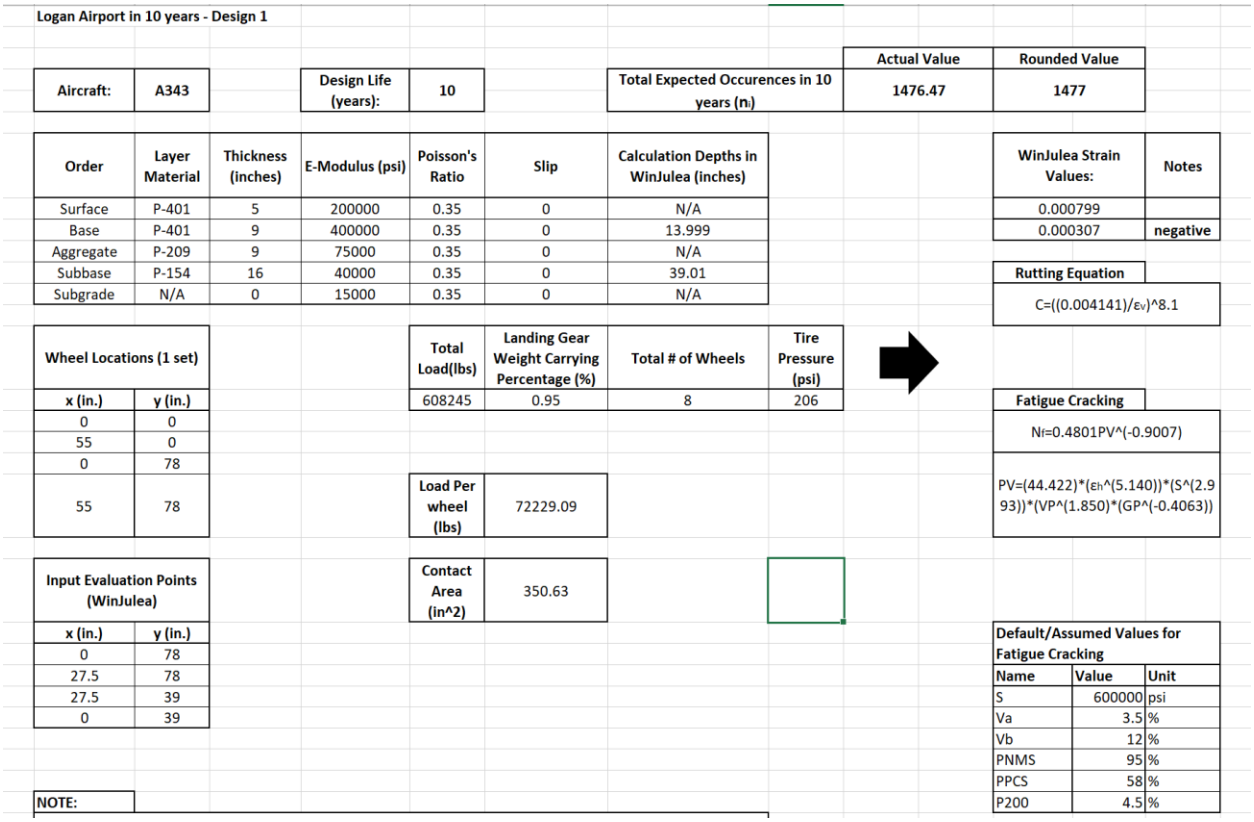

Logan Airport in 10 years - Design 1

Aircraft:	A343	Design Life (years):	10	Total Expected Occurences in 10 years (n_i)	Actual Value: 1476.47	Rounded Value: 1477

Order	Layer Material	Thickness (inches)	E-Modulus (psi)	Poisson's Ratio	Slip	Calculation Depths in WinJulea (inches)
Surface	P-401	5	200000	0.35	0	N/A
Base	P-401	9	400000	0.35	0	13.999
Aggregate	P-209	9	75000	0.35	0	N/A
Subbase	P-154	16	40000	0.35	0	39.01
Subgrade	N/A	0	15000	0.35	0	N/A

WinJulea Strain Values:	Notes
0.000799	
0.000307	negative

Rutting Equation

$C=((0.004141)/\varepsilon_v)^{8.1}$

Wheel Locations (1 set)	
x (in.)	y (in.)
0	0
55	0
0	78
55	78

Total Load(lbs)	Landing Gear Weight Carrying Percentage (%)	Total # of Wheels	Tire Pressure (psi)
608245	0.95	8	206

Load Per wheel (lbs)	72229.09

Contact Area (in^2)	350.63

Fatigue Cracking

$N_f=0.4801PV^{(-0.9007)}$

$PV=(44.422)*(\varepsilon_h^{(5.140)})*(S^{(2.993)})*(VP^{1.850})*(GP^{(-0.4063)})$

Input Evaluation Points (WinJulea)	
x (in.)	y (in.)
0	78
27.5	78
27.5	39
0	39

Default/Assumed Values for Fatigue Cracking

Name	Value	Unit
S	600000	psi
Va	3.5	%
Vb	12	%
PNMS	95	%
PPCS	58	%
P200	4.5	%

NOTE:

Figure 3-3: Design Starting Point

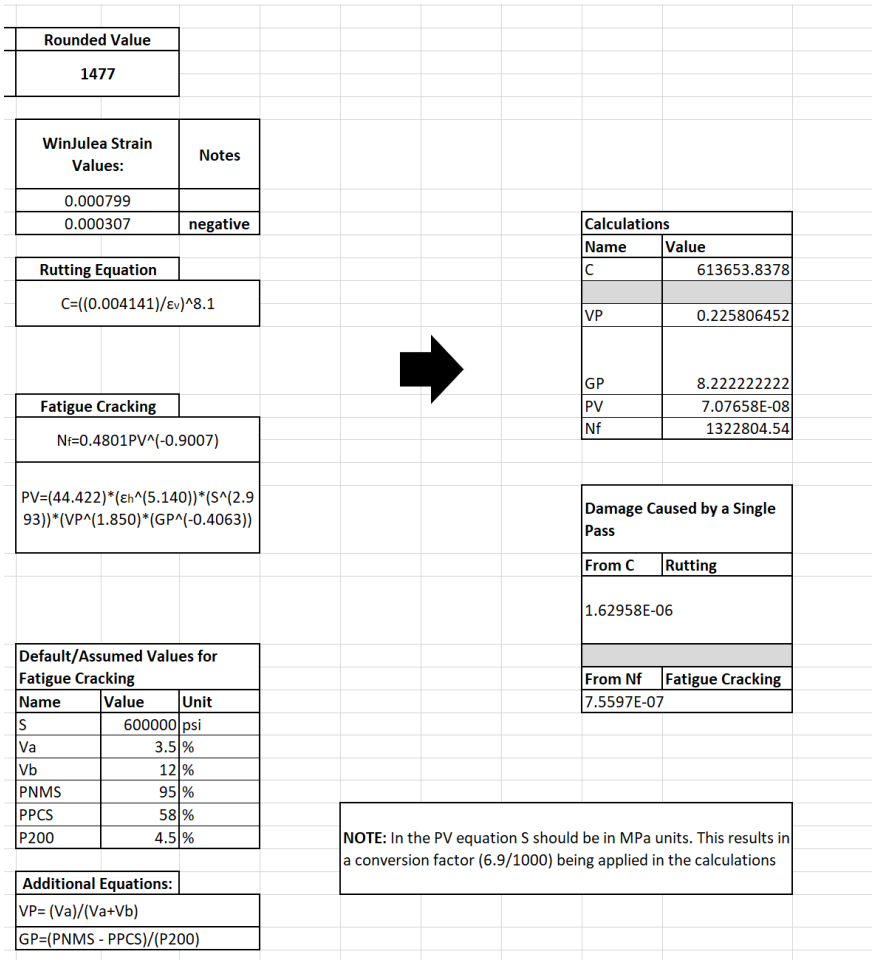

Rounded Value
1477

WinJulea Strain Values:	Notes
0.000799	
0.000307	negative

Rutting Equation
C=((0.004141)/εv)^8.1

Fatigue Cracking
Nf=0.4801PV^(-0.9007)
PV=(44.422)*(εh^(5.140))*(S^(2.993))*(VP^(1.850)*(GP^(-0.4063))

Default/Assumed Values for Fatigue Cracking		
Name	Value	Unit
S	600000	psi
Va	3.5	%
Vb	12	%
PNMS	95	%
PPCS	58	%
P200	4.5	%

Additional Equations:
VP= (Va)/(Va+Vb)
GP=(PNMS - PPCS)/(P200)

Calculations	
Name	Value
C	613653.8378
VP	0.225806452
GP	8.222222222
PV	7.07658E-08
Nf	1322804.54

Damage Caused by a Single Pass	
From C	Rutting
1.62958E-06	
From Nf	Fatigue Cracking
7.5597E-07	

NOTE: In the PV equation S should be in MPa units. This results in a conversion factor (6.9/1000) being applied in the calculations

Figure 3-4: Failure Calculations

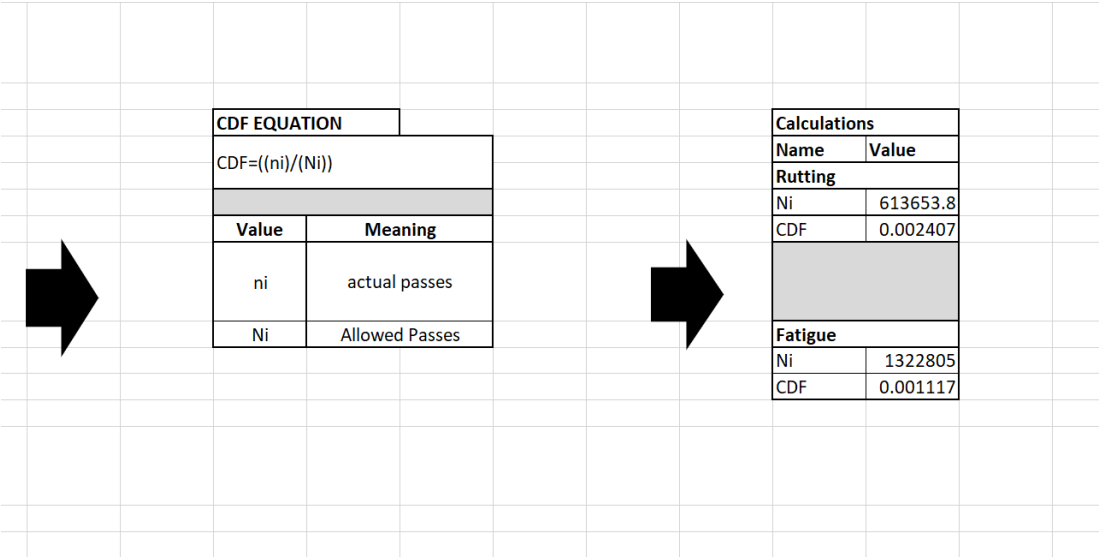

CDF EQUATION	
CDF=((ni)/(Ni))	
Value	Meaning
ni	actual passes
Ni	Allowed Passes

Calculations	
Name	Value
Rutting	
Ni	613653.8
CDF	0.002407
Fatigue	
Ni	1322805
CDF	0.001117

Figure 3-5: Results

Figure 3-6 was taken from Design 1 and shows the last sheet of the spreadsheet for that design where the individual CDF value from each aircraft was added together to get the final CDF for the design.

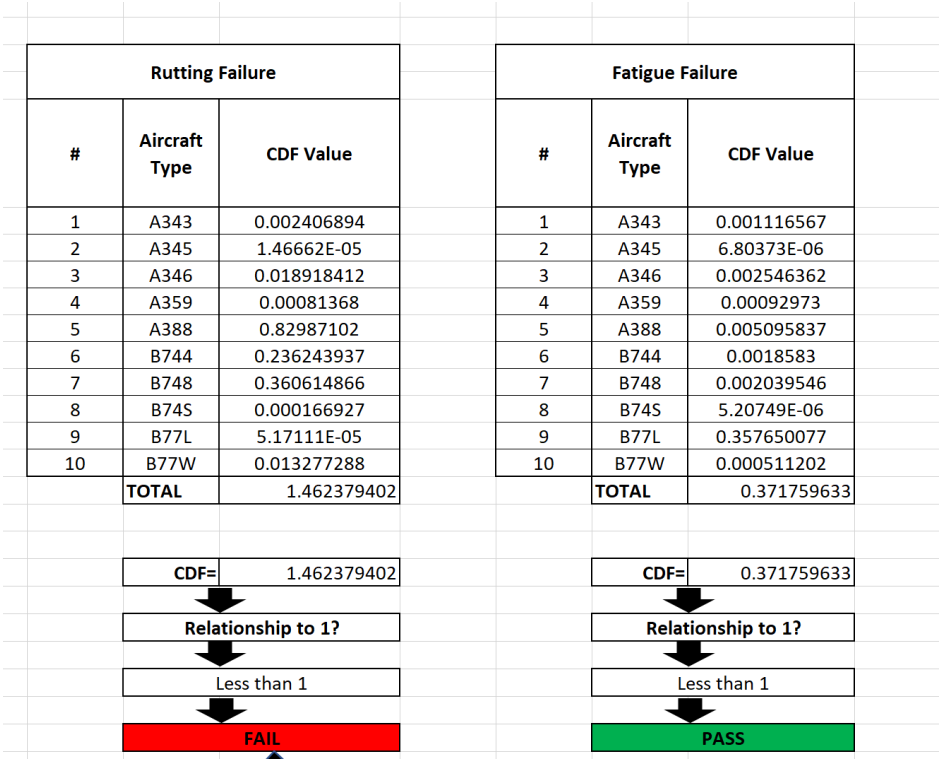

Rutting Failure		
#	Aircraft Type	CDF Value
1	A343	0.002406894
2	A345	1.46662E-05
3	A346	0.018918412
4	A359	0.00081368
5	A388	0.82987102
6	B744	0.236243937
7	B748	0.360614866
8	B74S	0.000166927
9	B77L	5.17111E-05
10	B77W	0.013277288
	TOTAL	1.462379402

Fatigue Failure		
#	Aircraft Type	CDF Value
1	A343	0.001116567
2	A345	6.80373E-06
3	A346	0.002546362
4	A359	0.00092973
5	A388	0.005095837
6	B744	0.0018583
7	B748	0.002039546
8	B74S	5.20749E-06
9	B77L	0.357650077
10	B77W	0.000511202
	TOTAL	0.371759633

Figure 3-6: Combining Aircraft CDF Values

3.4 Design Results

In this step of the design, the existing pavement structure was found to be under designed for the ten-year projected traffic, and hence a modification was needed. As this was an existing design, the surface layer was the only layer that could be changed, and this was the only modification that was considered in the design process. The design process resulted in an increase of thickness of the surface layer from 5 to 8 inch (Design 1.2). *Figure 3-7* and *Figure 3-8* show schematics of the original and the new pavement structure.

Design 1

Surface: P-401, Thickness: 5 inch

Base: P-401, Thickness: 9 inch

Aggregate: P-209, Thickness: 9 inch

Subbase: P-154, Thickness: 16 inch

Subgrade

Figure 3-7: Design 1 Schematic

Design 1.2

Surface: P-401, Thickness: 8 inch

Base: P-401, Thickness: 9 inch

Aggregate: P-209, Thickness: 9 inch

Subbase: P-154, Thickness: 16 inch

Subgrade

Figure 3-8: Design 1.2 Schematic

Table 3-2 lists the rutting and fatigue CDF values for the Logan Airport Design (design 1) and the successful design 1.2 – which was be used to test the future conditions.

Table 3-2: Cumulative Damage Factor for All Aircrafts in 10 years, Considering a Yearly 2% Growth

Design	Rutting CDF	Fatigue CDF
1	1.462379402	0.371759633
1.2	0.752554864	0.007579877

Figure 3-9 corresponds to the information presented in *Table 3-2*. From the figure, the difference between the two designs and their CDF value type results are visible. For design 1, the rutting CDF was well over 1. While the fatigue CDF value was not over 1 for design 1, the value is higher than design 1.2's value. Additionally, for both designs the factor that was controlling its failure was the rutting CDF as this value was the number closer to 1.

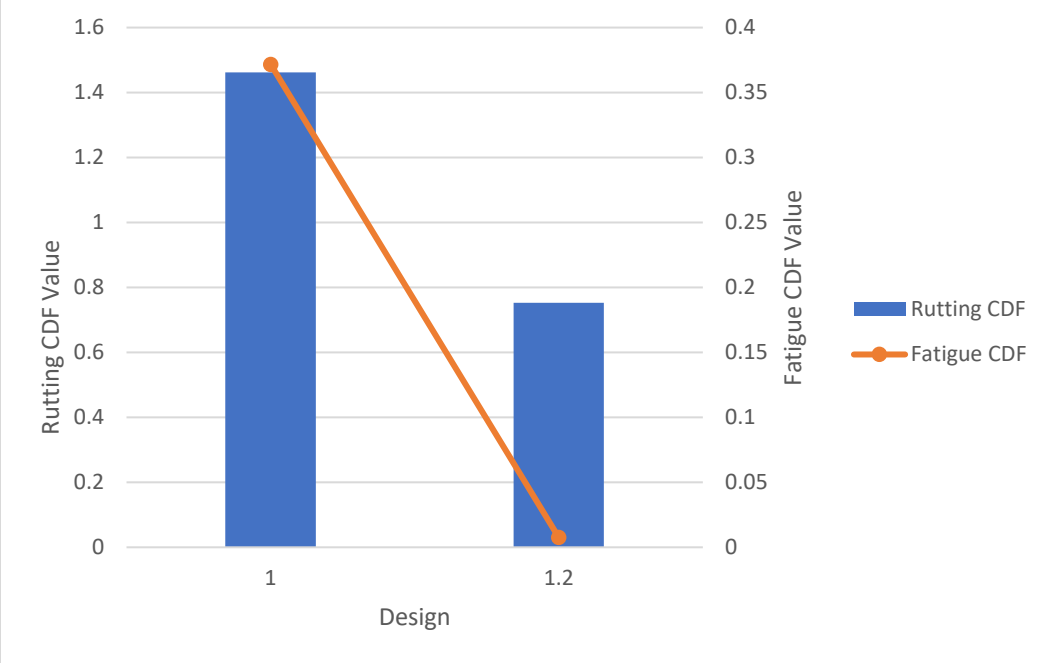

Figure 3-9: Comparison of Cumulative Damage Factor for All Aircrafts in 10 years, Considering a Yearly 2% Growth, between Two Designs

4.0 Design of Runway for Logan for Reduced Passenger Air Traffic and Increased Freight Air Traffic

Design 1.2 from *Chapter 3: Design of Runway for Boston Logan International Airport with Existing Air Traffic*, was used as the starting point for this chapter and all changes were done to the design created in the previous chapter. The design change that was applied in this chapter had the goal of increasing freight aircrafts and decreasing passenger aircrafts. These two goals were combined into one design by changing the B747-8 to a B777 and changing the A388 to an A350 and applying a five percent increase in the number of aircrafts for these smaller aircraft types. In this chapter no alterations were made to the pavement details. Changes were only applied to the aircrafts being used.

4.01 Design Schematics

As a reminder of the design layers, *Figure 4-1* shows the schematics for design 1.2.

Design 1.2

Surface: P-401, Thickness: 8 inch

Base: P-401, Thickness: 9 inch

Aggregate: P-209, Thickness: 9 inch

Subbase: P-154, Thickness: 16 inch

Subgrade

Figure 4-1: Design 1.2 Schematic

4.1 Application of Changes

In this design process the heavier aircrafts were replaced by smaller aircrafts and then a five percent increase was applied to account for freight traffic. The difference between the original aircraft and the replacement aircraft types were the wheel spacing, total number of wheels, the gross weight of the aircraft, and the tire pressure (USDOT: FAA, 2016b). These differences therefore created different strain values which result in different final rutting and fatigue CDF values for designs. The values shown in *Table 4-1* were the CDF values of design 1.2 with the described changes. With the five percent increase the total number of aircrafts used in this design was 11,274 (4.363% of 258, 378 – the original total).

Table 4-1: Cumulative Damage Factor for All Aircrafts in 10 years with 5% Increase Applied to the Overall Quantity of Two Aircraft Types (B777 and A350)

Rutting CDF	Fatigue CDF
0.136263238	0.003615849

The figure shown, *Figure 4-2*, corresponds to the data presented in *Table 4-1*. Similar to design 1 and design 1.2 from chapter 3, the pavement structure under this loading conditions will experience failure first in rutting as that value was closer to one – although it was well below 1 for the design life of 10 years.

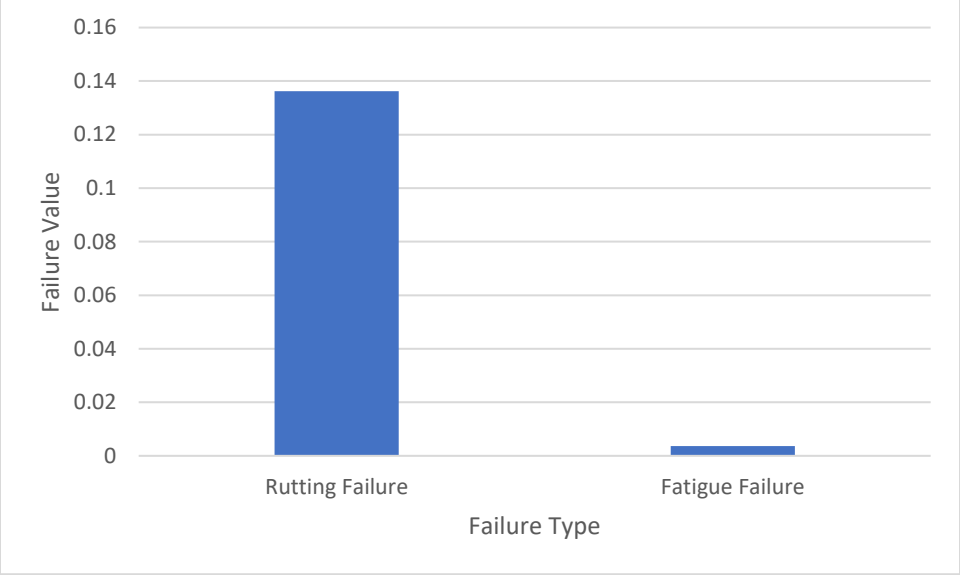

Figure 4-2: Comparison of Cumulative Damage Factors for Reduced Heavy and Increased Freight Aircrafts

5.0 Design of Runway for Logan International Airport with Predicted Traffic Plus 10% Supersonic Aircrafts

The goal of this design was to predict the impact supersonic aircrafts would have if the plans for their return proceed. In this step, the original design 1.2 (created in chapter 3) was considered with an additional supersonic aircraft. In the absence of any existing actual commercial supersonic aircrafts, the specific supersonic aircraft used for the additional 10% was the Concord as found in FAARFIELD (USDOT: FAA, 2016b). The 10% increase in design caused an increase in the total number of aircrafts to 13,323.

5.01 Design Schematics

Figure 5-1 shows the schematics for design 1.2.

Design 1.2

Surface: P-401, Thickness: 8 inch

Base: P-401, Thickness: 9 inch

Aggregate: P-209, Thickness: 9 inch

Subbase: P-154, Thickness: 16 inch

Subgrade

Figure 5-1: Design 1.2 Schematic

5.1 Effect of Supersonic Aircrafts

Table 5-1 contains the final CDF values for the designs considering the effects of supersonic aircraft damage. The difference in CDF values between these values and the original design CDF values were small.

Table 5 -1: Cumulative Damage Factor for Designs with an Additional 10% Quantity of Supersonic Aircrafts

Rutting CDF	Fatigue CDF
0.753404987	0.007789342

Figure 5-2 corresponds to the data presented in *Table 5-1*. As with the versions of design 1.2 in chapter 3 and chapter 4, the factor that would cause failure first for this design was the rutting failure. However, the design factors are still below 1 allowing the design to pass.

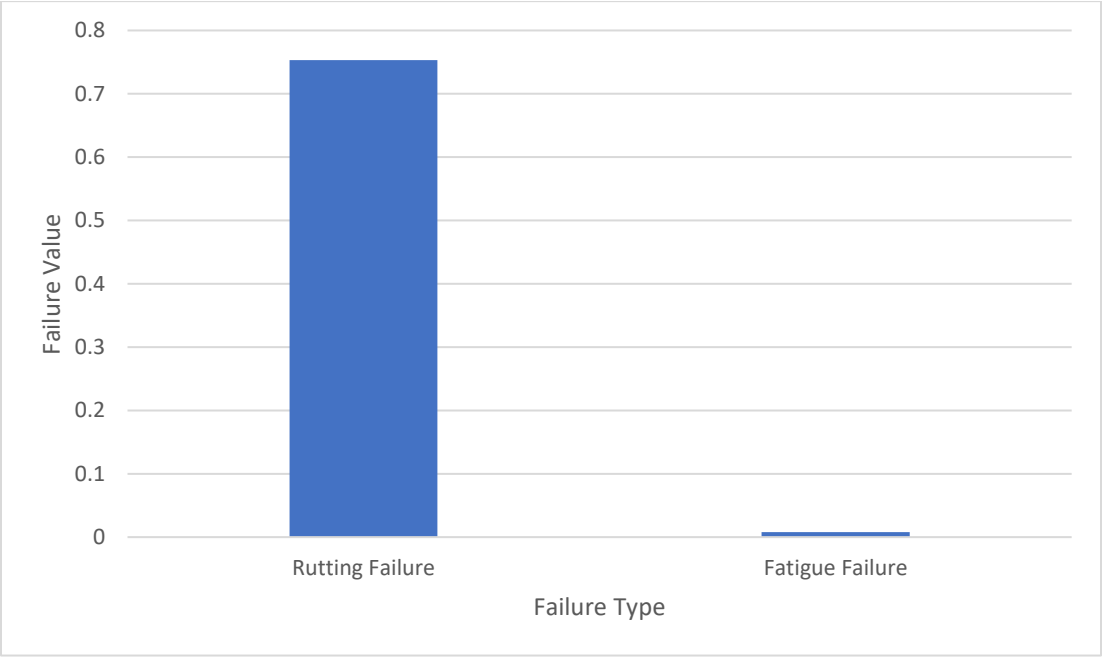

Figure 5-2: Comparison of Cumulative Damage Factors for Designs with an Additional 10% Supersonic Aircrafts

6.0 Design for Combination of Reduced Passenger, Increased Freight, and Supersonic Aircrafts

The goal of the design in this chapter was to take all conditions created in previous chapters and combine them together to create a design that could handle all future expected conditions post-COVID-19. As a result, the following design included all the variations in aircraft types and quantities.

6.01 Design Schematics

Figure 6-1 shows the schematics for design 1.2.

Design 1.2

Surface: P-401, Thickness: 8 inch

Base: P-401, Thickness: 9 inch

Aggregate: P-209, Thickness: 9 inch

Subbase: P-154, Thickness: 16 inch

Subgrade

Figure 6-1: Design 1.2 Schematic

6.1 Combination Effect

Table 6-1 shows the resulting CDF values from utilizing all aircraft alterations used in this MQP. These alterations were the addition of a supersonic aircraft, replacement aircraft types, and a five percent increase in quantity for two specific aircraft types (B777 and A350).

Table 6-1: Cumulative Damage Factor for All Expected Conditions

Rutting CDF	Fatigue CDF
0.137113362	0.003825314

The figure below, *Figure 6-2*, corresponds to the data presented in *Table 6-1*. As was evident with each of the versions of design 1.2, the rutting failure CDF was the closest to 1.

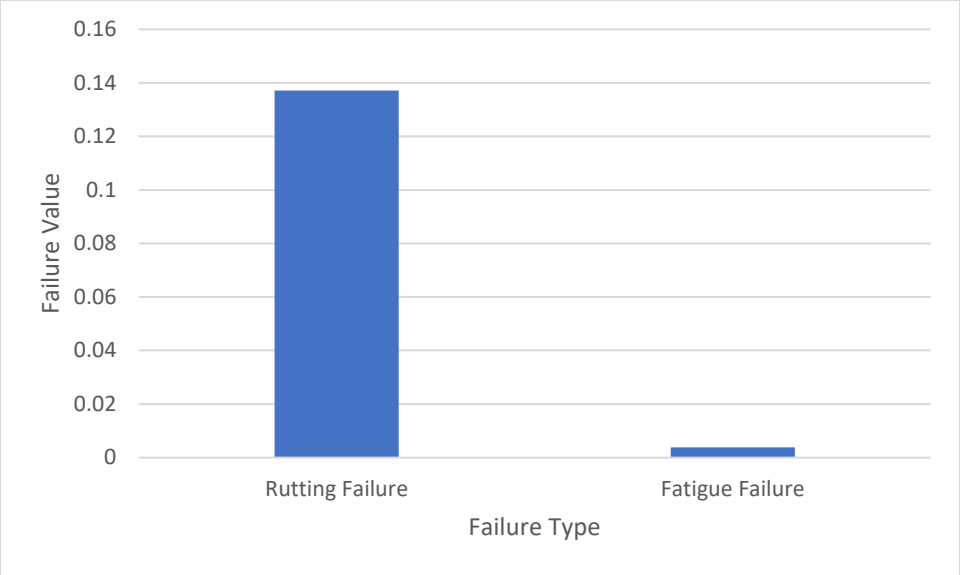

Figure 6.2: Comparison of Cumulative Damage Factor for Design with the Combination of all Changes in Air Traffic

7.0 Design Cost and Comparing Designs

The purpose of this chapter was to compare the different CDF values and estimate the cost of the designed pavement structure.

7.1 Material Pricing and Design Prices

Table 7-1 lists the costs of the different materials that were utilized to estimate the cost of the entire pavement structure from the subbase (S. Dennechuk, personal communication, March 8, 2021).

Table 7-1: Unit Pricing for Pavement Material (S. Dennechuk, personal communications, March 8, 2021)

Layer	Material	Units	Unit Price ($)
Surface	P-401	Tons	150.17
Base	P-401	Tons	153.17
Aggregate	P-209	CY	66.67
Subbase	P-154	CY	60.67

The following steps were conducted to calculate the total cost for each design. The example used in the steps was taken from the calculation of Design 1's cost:

Step 1: *Convert the layer's thickness units to feet*

12 inch = 1 foot

Thickness (inch)/ 12 inch = Thickness (feet)

Table 7-2: Layer Thickness Unit Conversion

Layer	Material	Thickness (in.)	Revised Thickness (ft.)
Surface	P-401	5	0.42
Base	P-401	9	0.75
Aggregate	P-209	9	0.75
Subbase	P-154	16	1.33
TOTAL		39	3.25

Step 2: *Calculate the volume of each layer* (FAA Information Effective 25 February 2021, n.d.)

Layer thickness x Length of Runway x Width of Runway = Volume (cubic feet)

Layer value x 7001 ft. x 150 ft. = Volume (cubic feet)

Table 7-3: Calculated Layer Volume

Layer	Thickness (ft.)	Length of Runway (ft.)	Width of Runway (ft.)	Volume (cubic feet)
Surface	0.42	7001	150	437562.5
Base	0.75	7001	150	787612.5
Aggregate	0.75	7001	150	787612.5
Subbase	1.33	7001	150	1400200

TOTAL	3.25	7001	150	3412987.5

Step 3: *Convert volume to yards and tons – if needed* (Convert Ton Register to Cubic Yard, n.d.)

1 yard = 3 feet

1 cubic yard = 3 ft. x 3 ft. x 3ft. = 27 cubic feet

Volume (cubic feet)/ 27 cubic feet = Volume (cubic yard)

1 ton = 3.703 cubic yards

Volume (cubic yard)/ 3.703 cubic yard = Volume (tons)

Table 7-4: Layer Volume Unit Conversions

Layer	Volume (cubic feet)	Volume (cubic yards)	Volume (tons)
Surface	437562.5	16206.02	4376.457
Base	787612.5	29170.83	7877.622
Aggregate	787612.5	29170.83	N/A
Subbase	1400200	51859.26	N/A
TOTAL	3412987.5	126406.9	N/A

Step 4: *Price for layer*

Volume (tons) x Unit price for layer = layer price OR

Volume (cubic yard) x Unit price for layer = layer price

Table 7-5: Calculated Layer Price and Total Price

Layer	Volume (cubic yards)	Volume (tons)	Unit Price ($)	Price ($)
Surface	16206.02	4376.457	150.17	657197.9
Base	29170.83	7877.622	153.17	1206589
Aggregate	29170.83	N/A	66.67	1944722
Subbase	51859.26	N/A	60.67	3146128
TOTAL	126406.9	N/A	N/A	**6954638**

Step 5: *Total Price*

Summing all the Layer prices together = Total Price

Table 7-2 shows the overall cost for design 1 and design 1.2. Although design 1 was unusable as it had initially failed, the cost is included for comparison to show how much of a price difference an additional three inches of P-401 material can cause.

Table 7-6: Comparison of Overall Design Cost Based on Material Pricing

Design	Overall Cost for the Entire Runway
1	$6,954,637.60
1.2	$7,348,956.30

7.2 Comparison Between Designs

Table 7-3 shows the CDF values for all the variations of the designs that were considered in this MQP. Ignoring design 1's CDF values as this design failed, the two designs with the highest CDF values was the initial pre-COVID-19 design 1.2 and the design 1.2 that had the conditions of pre-COVID-19 and supersonic air traffic, both of these high values were associated with the rutting failure of the design. Of all the design variations, design 1.2 that considered an increased freight and decreased passenger traffic had the lowest CDF values. The final Design 1.2 was the only design that considers every condition and has the second lowest CDF values.

Table 7-7: Compilation of Cumulative Damage Factors

Design	Structure	Rutting CDF	Fatigue CDF
Design 1: Logan Airport Pre-COVID-19	5 inch of surface P-401	1.46	0.37
Design 1.2: Logan Airport Pre-COVID-19	8 inch of surface P-401	0.75	07.57×10^{-3}
Design 1.2: Increased Freight and Decreased Passenger Traffic	8 inch of surface P-401	0.13	3.61×10^{-3}
Design 1.2: Pre-COVID-19 and Supersonic Traffic	8 inch of surface P-401	0.75	7.78×10^{-3}
Design 1.2: All Combinations	8 inch of surface P-401	0.13	3.82×10^{-3}

Figure 7-1 corresponds to the data presented in *Table 7-3.*

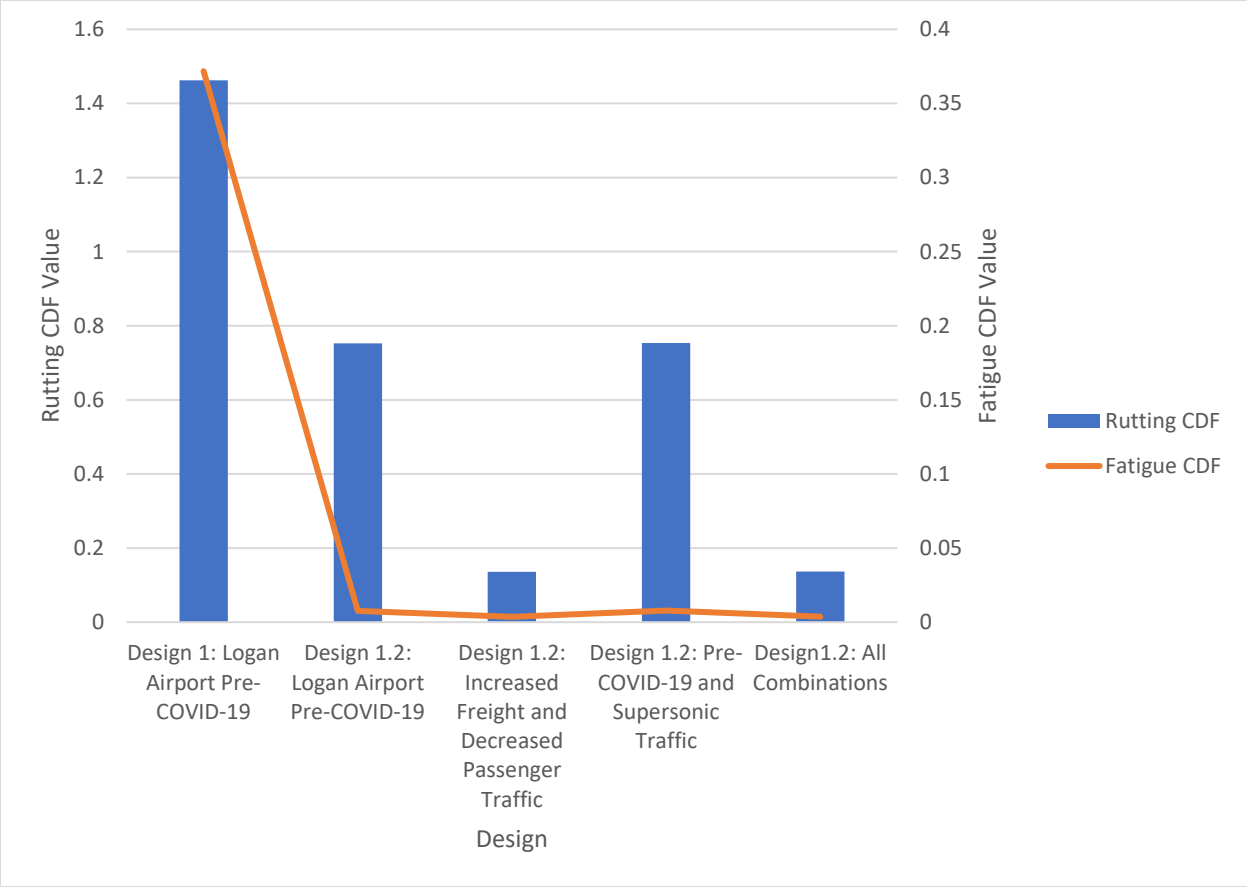

Figure 7-1: Comparison of Compilation of Cumulative Damage Factors

8.0 Summary

Departure data from Logan International Airport from 2019 was applied a two percent yearly growth for ten years to get a final cumulative number of aircrafts taken off. From this information, the ten aircrafts with highest taxi load were used as the influencing aircrafts for designing a runway pavement with a consideration of post-COVID-19 conditions. Considering multiple runways, a third of the air traffic was utilized for the design of a single runway asphalt pavement. Mechanistic-empirical analyses were conducted with the help of layered elastic analysis. The four specific cases that were considered for the design are as follows: pre-COVID-19 traffic, increased freight and decreased passenger air traffic, pre-COVID-19 and supersonic traffic, and a combination of all the conditions. *Figure 8-1* presents the details of the pavement design that passed all air traffic conditions. The cost for this design, Design 1.2, was $7,348,956.30 (for the entire runway) for a volume of 136,130.56 cubic yards, based on current pricing being used at Logan International Airport for runway repair.

Design 1.2

Surface: P-401, Thickness: 8 inch

Base: P-401, Thickness: 9 inch

Aggregate: P-209, Thickness: 9 inch

Subbase: P-154, Thickness: 16 inch

Subgrade

Figure 8-1: Design 1.2 Schematic

References

Abbot, B. (2014). Boeing 777 Eva Air letdown DSC_0004 [Photograph]. *flickr*. https://www.flickr.com/photos/wbaiv/14578610947

Airbus. (n.d.). *A350-900.* https://www.airbus.com/aircraft/passenger-aircraft/a350xwb-family/a350-900.html

Boeing. (n.d.). *Boeing: 777* [Timeline of changes to aircraft]. Retrieved October, 2020 from https://www.boeing.com/commercial/777/#/design-highlights/technology/product-improvements/

Boom Supersonic. (2019, September 17). *The Big 3 Components of Supersonic Aircraft*. Medium. https://blog.boomsupersonic.com/the-big-3-components-of-supersonic-aircraft-c1c614aeedbb

Boom Supersonic. (2020, June 4). *Tomorrow's Air Travel is Supersonic and Sustainable*. Medium. https://blog.boomsupersonic.com/tomorrows-air-travel-is-supersonic-and-sustainable-12e39244dbce

Boom Supersonic. (n.d.) [Conceptual Image of Supersonic Aircraft]. [Design Photograph]. *Boom Supersonic.* https://boomsupersonic.com/

Boston Logan Airport. (n.d.) Boston Airport: Guide to Boston Logan International Airport (BOS). Retrieved October 12, 2020, from https://www.boston-airport.com/

Boyd, I. (2019, July 11). *Commercial supersonic aircraft could return to the skies*. The Conversation. https://theconversation.com/commercial-supersonic-aircraft-could-return-to-the-skies-113022

Centers for Disease Control and Prevention. (2020). *About COVID – 19.* https://www.cdc.gov/coronavirus/2019-ncov/cdcresponse/about-COVID-19.html

Climate – Boston (Massachusetts). (n.d.). Climates To Travel World Climate Guide. Retrieved February 10, 2021, from https://www.climatestotravel.com/climate/united-states/boston#:~:text=Precipitation%20in%20Boston%20is%20quite,well%20distributed%20over%20the%20seasons.

Convert Ton Register to Cubic Yard. (n.d.). UnitConverters.net. Retrieved March 10, 2021, from https://www.unitconverters.net/volume/ton-register-to-cubic-yard.htm

Cummins, N. (2020, September 22). *Why is Airbus Yet to Conquer the Freight Market.* Simple Flying. https://simpleflying.com/airbus-freight-market/

Emirates. (n.d.). *COVID-19 response: Emirates SkyCargo to set up the world's largest GDP compliant air cargo hub in Dubai for global distribution of COVID-19 vaccine.* Emirates. https://www.emirates.com/media-centre/covid-19-response-emirates-skycargo-to-set-up-the-worlds-largest-gdp-compliant-air-cargo-hub-in-dubai-for-global-distribution-of-covid-19-vaccine

Engineering Research & Development Center [ERDC – WES]. (n.d.). *WinJulea*. Engineering Research & Development Center [ERDC – WES].

FAA Information Effective 25 February 2021. (n.d.). AirNav.com. Retrieved March 10, 2021, from https://www.airnav.com/airport/KBOS

Google. (n.d.). [Google Map of Boston Logan International Airport]. Retrieved March 19, 2021, from https://www.google.com/maps/place/Boston+Logan+International+Airport/@42.3658775,-71.0182858,4839m/data=!3m1!1e3!4m5!3m4!1s0x89e37014d5da4937:0xc9394c31f2d5144!8m2!3d42.3656132!4d-71.0095602?hl=en

Iacus, S., Natale, F., Santamaria, C., Spyratos, S., & Vespe, M. (2020). Estimating and projecting air passenger traffic during the COVID-19 coronavirus outbreak and its socio-economic impact. *Safety Science*, 129, 104791–. https://doi.org/10.1016/j.ssci.2020.104791

Icarus, A. (2020). Air China Airbus A350-900; B-1080@FRA;09.07.2020 [Photograph]. *flickr*. https://www.flickr.com/photos/aero_icarus/50105616171

Josephs, L. (2019, June 17). *Rome to New York in a narrowbody jet? Airbus launches a lean new plane for long flights*. CNBC. https://www.cnbc.com/2019/06/17/airbus-bets-on-smaller-jets-for-long-flights-with-new-a321xlr.html

Kulisch, E. (2020, October 12). *Asiana reconfigures A350 passenger cabin with Airbus cargo pallet system.* American Shipper. https://www.freightwaves.com/news/asiana-reconfigures-a350-passenger-cabin-with-new-airbus-cargo-pallet-system

Lappin, T. (2007). Airbus A380 at SFO [Photograph]. flickr. https://www.flickr.com/photos/telstar/1486068582

Logan International Airport (BOS), Boston, MA, USA. (n.d.). LatLong.net. Retrieved March 19, 2021, from https://www.latlong.net/place/logan-international-airport-bos-boston-ma-usa-1815.html

Mallick, R., & El-Korchi, T. (2017). *Pavement Engineering: Principles and Practice* (Third Edition). Milton: Taylor & Francis Group.

Nahum, O., Hadas, Y., & Kalish, A. (2019). A Combined Freight and Passenger Planes Cargo Allocation Model. *Transportation Research Procedia*, 37, 354–361. https://doi.org/10.1016/j.trpro.2018.12.203

Oertle, M. (2014a). Lufthansa Cargo McDonnell Douglas MD-11F D-ALCK [Photograph]. *flickr*. https://www.flickr.com/photos/kambui/37587203236/

Oertle, M. (2014b). Saudi Arabian Airlines Cargo (Air Atlanta Icelandic) Boeing 747-481(BCF) TF-AMP [Photograph]. flickr. https://www.flickr.com/photos/kambui/26034053640/

Personal Communications with Sarah Dennechuk Senior Project Manager for the Massachusetts Port Authority, October 7, 2020.

Personal Communications with Sarah Dennechuk Senior Project Manager for the Massachusetts Port Authority, October 30, 2020.

Personal Communications with Sarah Dennechuk Senior Project Manager for the Massachusetts Port Authority, March 8, 2021.

Proactive Investors: Boeing ups its 20-year industry forecast for passenger and freight planes demand by 4. (2017). In *Newstex Finance & Accounting Blogs*. Newstex.

Smith, J. (2020, March 20). Passenger Airlines Start Shifting Idled Planes Into Freight Business. *The Wall Street Journal*. https://www.wsj.com/articles/passenger-airlines-start-shifting-idled-planes-into-freight-business-11584737793

Suau-Sanchez, P., Voltes-Dorta, A., & Cugueró-Escofet, N. (2020). An early assessment of the impact of COVID-19 on air transport: Just another crisis or the end of aviation as we know it?. *Journal of transport geography*, *86*, 102749. https://doi.org/10.1016/j.jtrangeo.2020.102749

Turner, J. (2020, January 23). *Sonic boom: do airports need to prepare for the supersonic revolution?.* Airport Technology. https://www.airport-technology.com/features/supersonic-passenger-aircraft/

United States Department of Transportation: Federal Aviation Administration. (2016a). *AC 150/5320-6F – Airport Pavement Design and Evaluation.* https://www.faa.gov/documentLibrary/media/Advisory_Circular/150-5320-6F.pdf

United States Department of Transportation: Federal Aviation Administration. (2016b) *FAARFIELD* (Version 1.42). United States Department of Transportation: Federal Aviation Administration. https://www.airporttech.tc.faa.gov/Products/Airport-Pavement-Software-Programs/Airport-Software-Detail/ArtMID/3708/ArticleID/4/FAARFIELD-142

United States Department of Transportation: Federal Aviation Administration. (2020). *Fact Sheet – Supersonic Flight.* https://www.faa.gov/news/fact_sheets/news_story.cfm?newsId=22754

Walton, J. (2020, April 22). *Will empty middle seats help social distancing on planes?*. BBC. https://www.bbc.com/worklife/article/20200422-when-can-we-start-flying-again

World Health Organization. (2020). *Timeline: WHO's COVID – 19 response.* [Data and Timeline]. World Health Organization. Retrieved October 5, 2020, from https://www.who.int/emergencies/diseases/novel-coronavirus-2019/interactive-timeline?gclid=EAIaIQobChMIpOjA26ec7AIVwZzCh0LywJVEAMYASAAEgJOMPD_BwE#event-71

Shen, S., & Carpenter, S., (2007). Development of an Asphalt Fatigue Model Based on Energy Principles. Journal of the Association of Asphalt Paving Technologists, vol. 76, 533.

Appendix

Appendix A: Example of Logan Airport 2019 Air Traffic Data

Aircraft Type	Gross Taxi Weight (lbs)	Tire Pressure (psi)	Surface Area that touches Pavement (in^	# Occurences in 2019	2% growth (2020)	2% growth (2021)	2% growth (2022)	2% growth (2023)	2% growth (2024)	2% growth (2025)	2% growth (2026)	2% growth (2027)	2% growth (2028)	2% growth (2029)	Note (name in FAARFIELD):
737				2	2.04	2.08	2.12	2.16	2.21	2.25	2.30	2.34	2.39	2.44	
A109				7	7.14	7.28	7.43	7.58	7.73	7.88	8.04	8.20	8.37	8.53	
A139				132	134.64	137.33	140.08	142.88	145.74	148.65	151.63	154.66	157.75	160.91	
A20N				32	32.64	33.29	33.96	34.64	35.33	36.04	36.76	37.49	38.24	39.01	
A21N				700	714.00	728.28	742.85	757.70	772.86	788.31	804.08	820.16	836.56	853.30	
A306	380518	194	232.5	1067	1088.34	1110.11	1132.31	1154.96	1178.05	1201.62	1225.65	1250.16	1275.16	1300.67	A300-600 std.
A319	141,978	173	195.36	8134	8296.68	8462.61	8631.87	8804.50	8980.59	9160.21	9343.41	9530.28	9720.88	9915.30	A319-100 std.
A320	150,796	200	178.94	29981	30580.62	31192.23	31816.08	32452.40	33101.45	33763.48	34438.75	35127.52	35830.07	36546.67	A320-100
A321	183,866	197	221.38	22728	23182.56	23646.21	24119.14	24601.52	25093.55	25595.42	26107.33	26629.47	27162.06	27705.31	A321-100 std.
A332	509047	206	293.52	1083	1104.66	1126.75	1149.29	1172.27	1195.72	1219.63	1244.03	1268.91	1294.29	1320.17	A330-200 std
A333	509047	206	293.52	2883	2940.66	2999.47	3059.46	3120.65	3183.06	3246.73	3311.66	3377.89	3445.45	3514.36	A330-300 std
A339				136	138.72	141.49	144.32	147.21	150.15	153.16	156.22	159.35	162.53	165.78	
A340	568,563	191	289.63	1	1.02	1.04	1.06	1.08	1.10	1.13	1.15	1.17	1.20	1.22	A340-200 std.
A343	608245	206	287.88	364	371.28	378.71	386.28	394.01	401.89	409.92	418.12	426.48	435.01	443.71	A340-300 std.
A345	813947	234	286.92	2	2.04	2.08	2.12	2.16	2.21	2.25	2.30	2.34	2.39	2.44	A340-500 std.
A346	807333	234	284.01	313	319.26	325.65	332.16	338.80	345.58	352.49	359.54	366.73	374.06	381.55	A340-600 std.
A359	601650	241	296.46	250	255.00	260.10	265.30	270.61	276.02	281.54	287.17	292.91	298.77	304.75	A350-900
A388	1238998	218	270.46	353	360.06	367.26	374.61	382.10	389.74	397.54	405.49	413.60	421.87	430.31	A380
A400	289,687	133	172.43	1	1.02	1.04	1.06	1.08	1.10	1.13	1.15	1.17	1.20	1.22	A400M TLL 1
A76				1	1.02	1.04	1.06	1.08	1.10	1.13	1.15	1.17	1.20	1.22	
AA5				1	1.02	1.04	1.06	1.08	1.10	1.13	1.15	1.17	1.20	1.22	

Figure A-1: Example of Logan Airport 2019 Air Traffic Data

Appendix B: Design 1.2

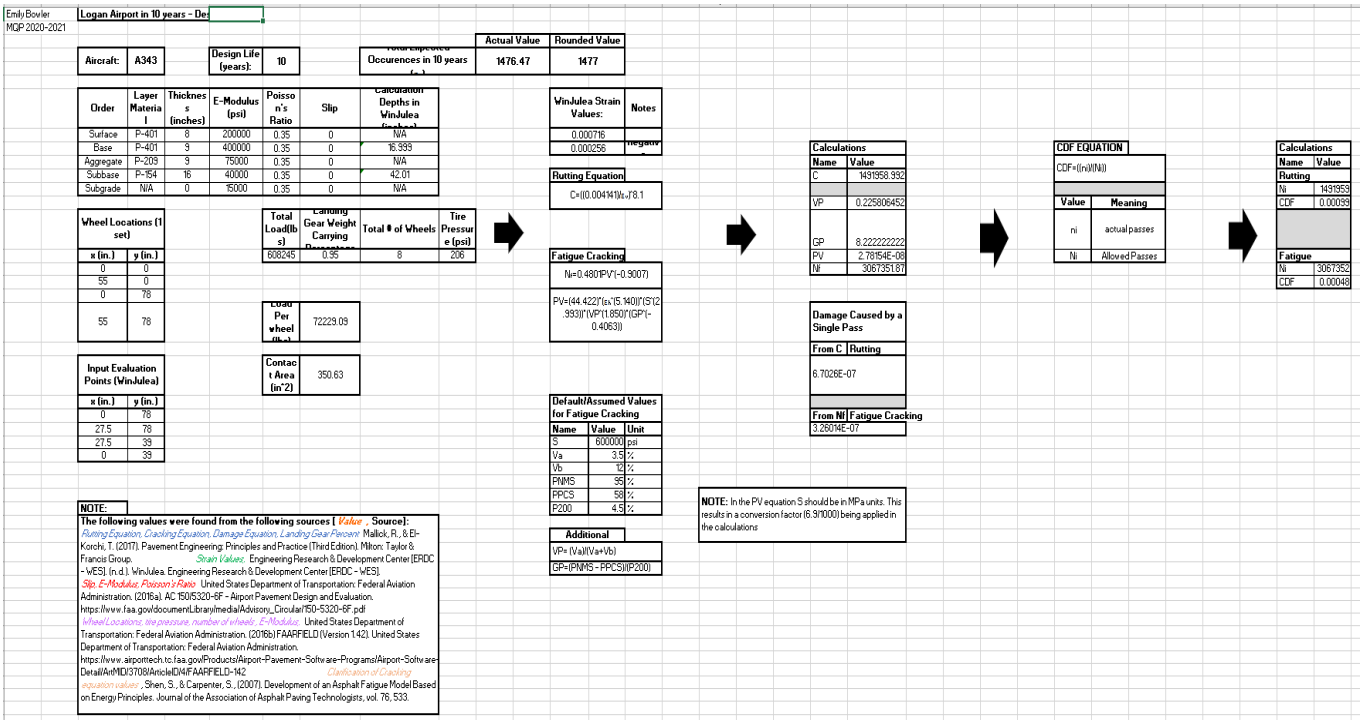

Figure B-1: Design 1.2 Aircraft A343

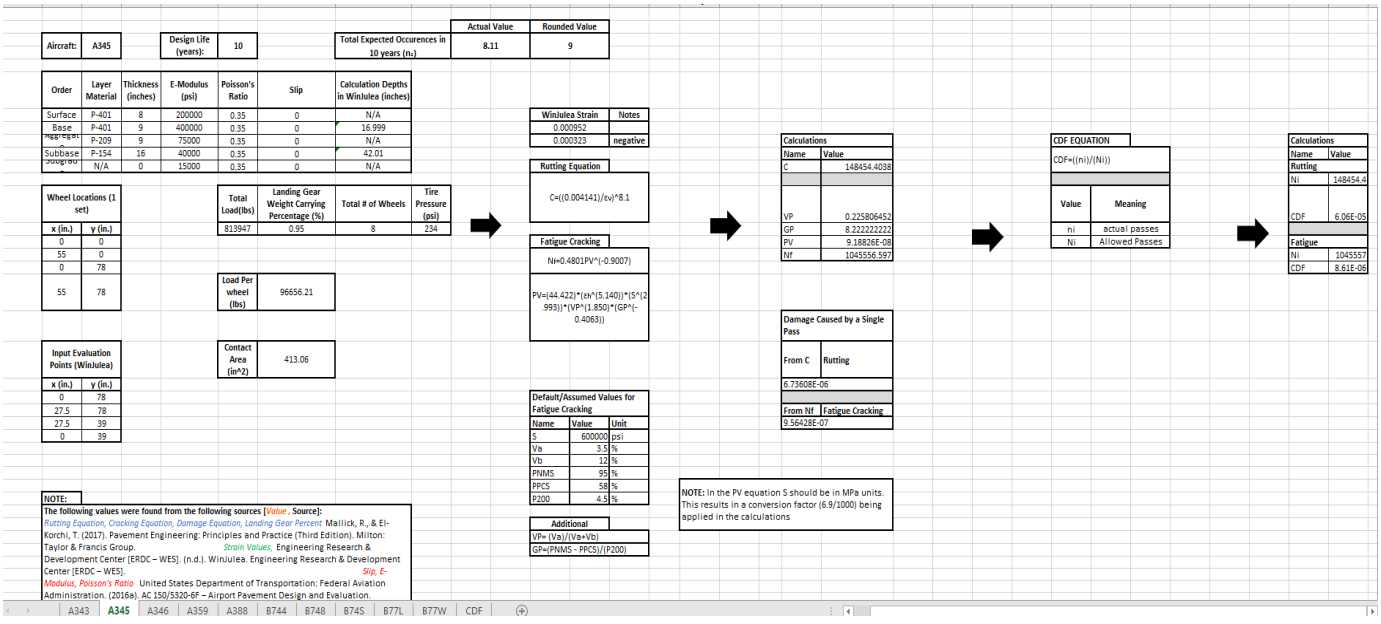

Figure B-2: Design 1.2 Aircraft A345

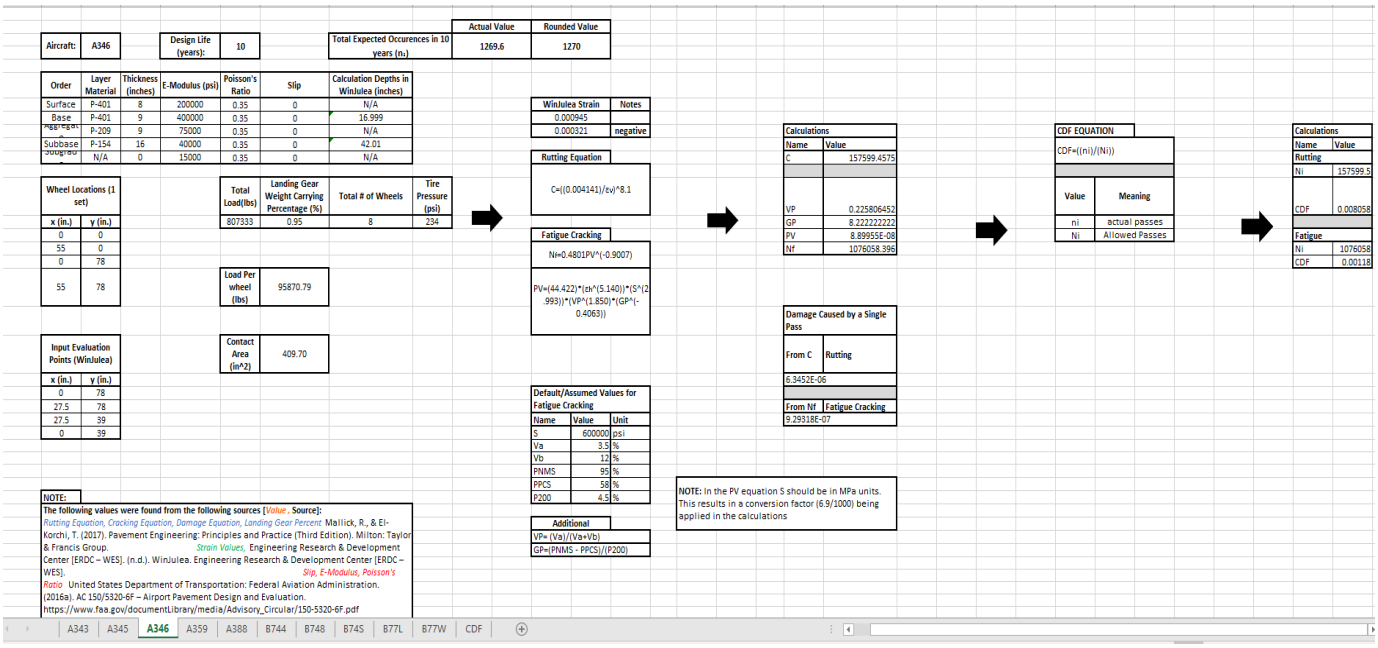

Figure B-3: Design 1.2 Aircraft A346

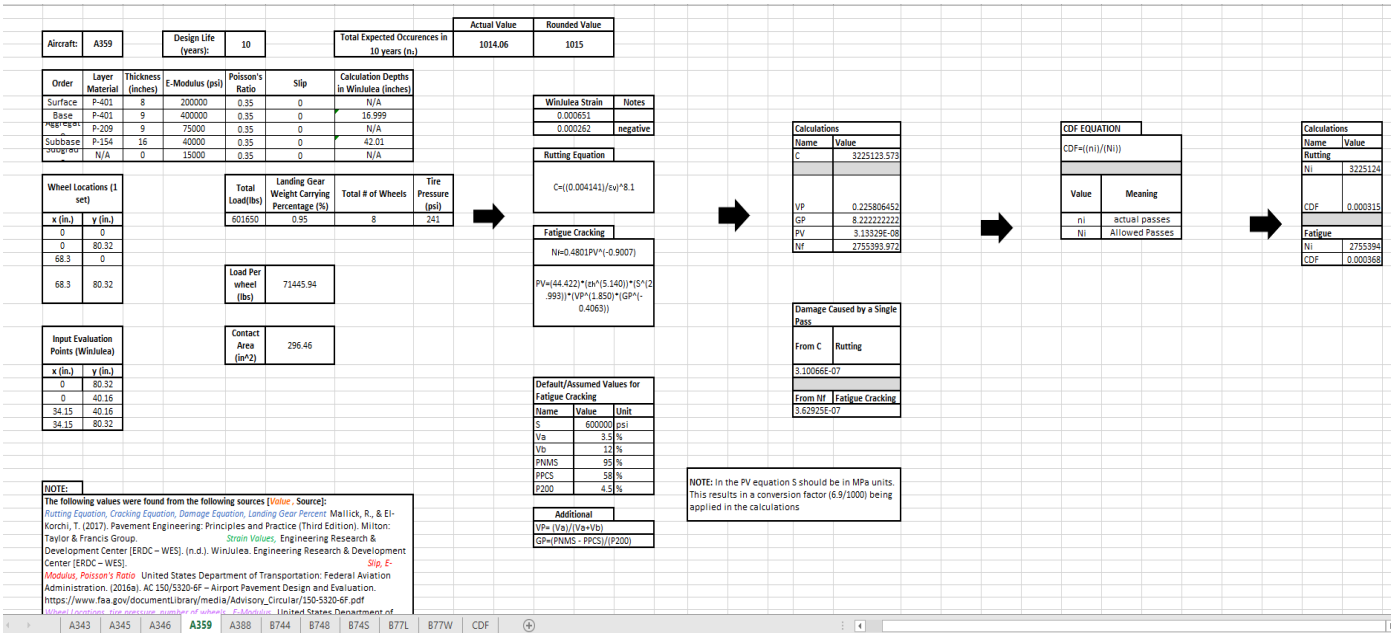

Figure B-4: Design 1.2 Aircraft A359

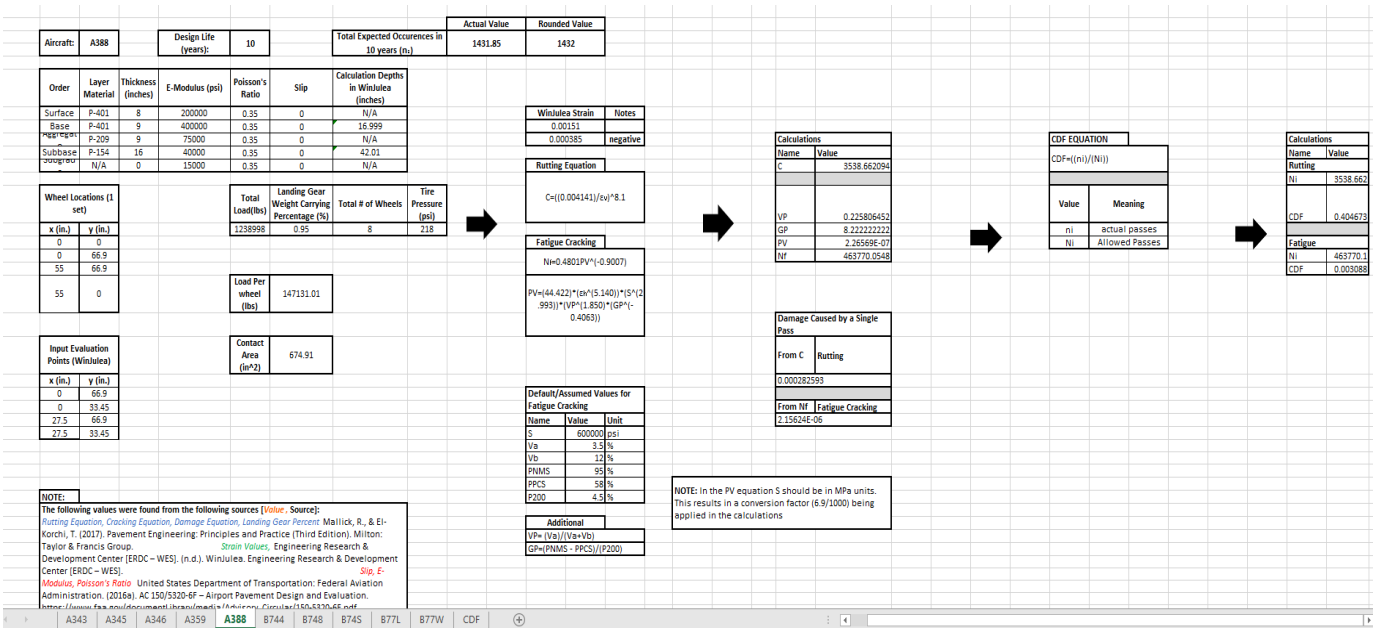

Figure B-5: Design 1.2 Aircraft A388

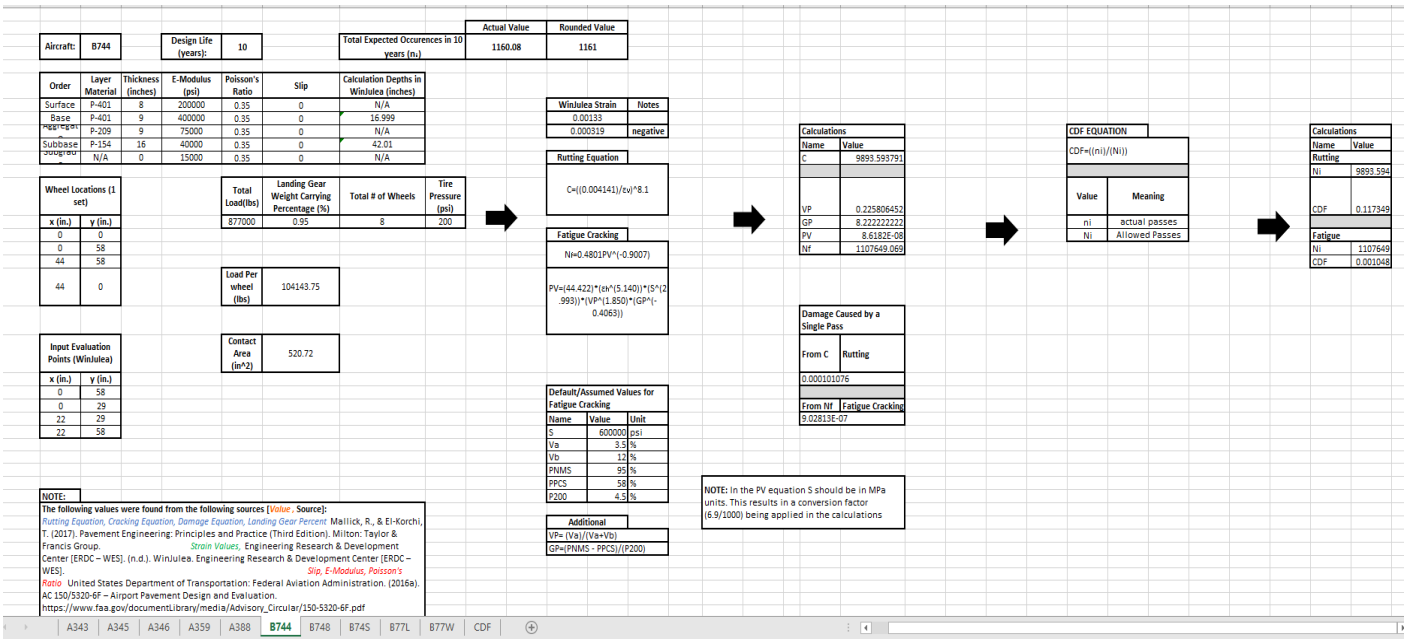

Figure B-6: Design 1.2 Aircraft B744

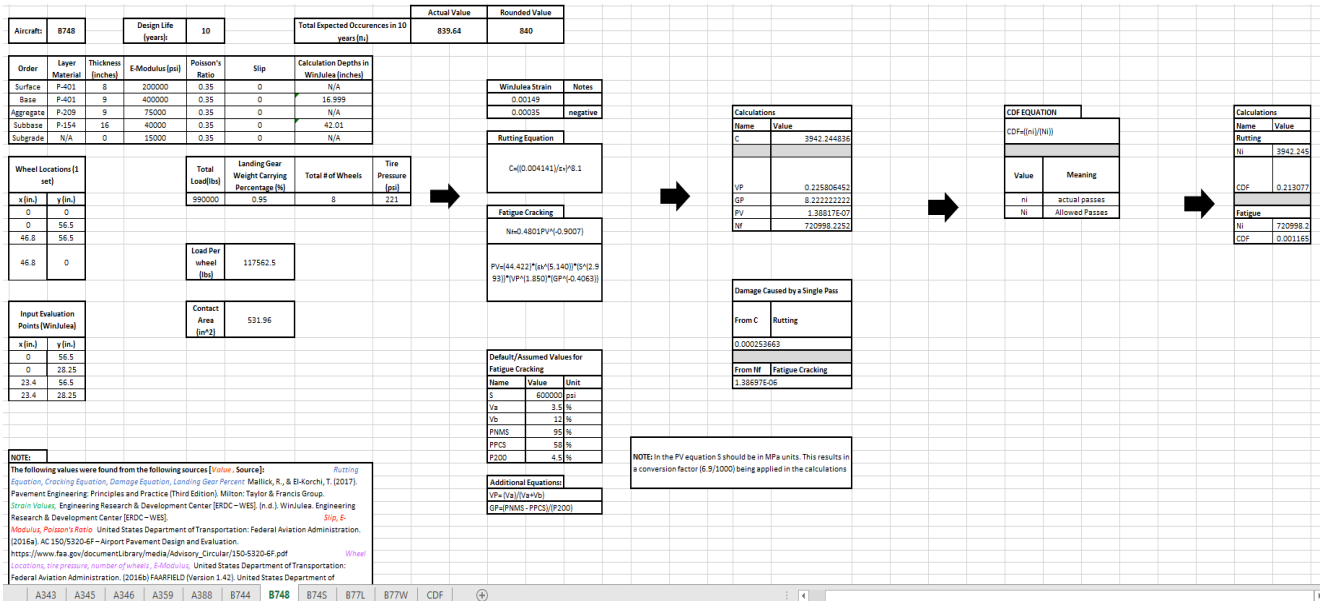

Aircraft:	B748
Design Life (years):	10
Total Expected Occurences in 10 years (n_t)	Actual Value: 839.64 / Rounded Value: 840

Order	Layer Material	Thickness (inches)	E-Modulus (psi)	Poisson's Ratio	Slip	Calculation Depths in WinJulea (inches)
Surface	P-401	8	200000	0.35	0	N/A
Base	P-401	9	400000	0.35	0	16.999
Aggregate	P-209	9	75000	0.35	0	N/A
Subbase	P-154	16	40000	0.35	0	42.01
Subgrade	N/A	0	15000	0.35	0	N/A

Wheel Locations (1 set)	
x (in.)	y (in.)
0	0
0	56.5
46.8	56.5
46.8	0

Total Load(lbs)	Landing Gear Weight Carrying Percentage (%)	Total # of Wheels	Tire Pressure (psi)
990000	0.95	8	221

Load Per wheel (lbs)	117562.5
Contact Area (in^2)	531.96

Input Evaluation Points (WinJulea)	
x (in.)	y (in.)
0	56.5
0	28.25
23.4	56.5
23.4	28.25

WinJulea Strain	Notes
0.00149	
0.00035	negative

Rutting Equation

C=((0.004141)/ε)^8.1

Fatigue Cracking

Nf=0.4801PV^(-0.9007)

PV=(44.422)*(εt^(5.140))*(S^(2.993))*(VP^(1.850)*(GP^(-0.4063))

Default/Assumed Values for Fatigue Cracking		
Name	Value	Unit
S	600000	psi
Va	3.5	%
Vb	12	%
PNMS	95	%
PPCS	58	%
P200	4.5	%

Additional Equations:

VP= (Va)/(Va+Vb)

GP=(PNMS - PPCS)/(P200)

Calculations	
Name	Value
C	3942.244836
VP	0.225806452
GP	8.222222222
PV	1.38817E-07
Nf	720998.2252

Damage Caused by a Single Pass	
From C	Rutting
0.000253663	
From Nf	Fatigue Cracking
1.38697E-06	

NOTE: In the PV equation S should be in MPa units. This results in a conversion factor (6.9/1000) being applied in the calculations

CDF EQUATION	
CDF=((ni)/(Ni))	
Value	Meaning
ni	actual passes
Ni	Allowed Passes

Calculations	
Name	Value
Rutting	
Ni	3942.245
CDF	0.213077
Fatigue	
Ni	720998.2
CDF	0.001165

NOTE:
The following values were found from the following sources [*Value* , **Source**]:
Rutting Equation, Cracking Equation, Damage Equation, Landing Gear Percent Mallick, R., & El-Korchi, T. (2017). Pavement Engineering: Principles and Practice (Third Edition). Milton: Taylor & Francis Group.
Strain Values, Engineering Research & Development Center [ERDC – WES]. (n.d.). WinJulea. Engineering Research & Development Center [ERDC – WES].
Slip, E-Modulus, Poisson's Ratio United States Department of Transportation: Federal Aviation Administration. (2016a). AC 150/5320-6F – Airport Pavement Design and Evaluation. https://www.faa.gov/documentLibrary/media/Advisory_Circular/150-5320-6F.pdf
Wheel Locations, tire pressure, number of wheels , E-Modulus, United States Department of Transportation: Federal Aviation Administration. (2016b) FAARFIELD (Version 1.42). United States Department of

A343 | A345 | A346 | A359 | A388 | B744 | B748 | B74S | B77L | B77W | CDF

Figure B-7: Design 1.2 Aircraft B748

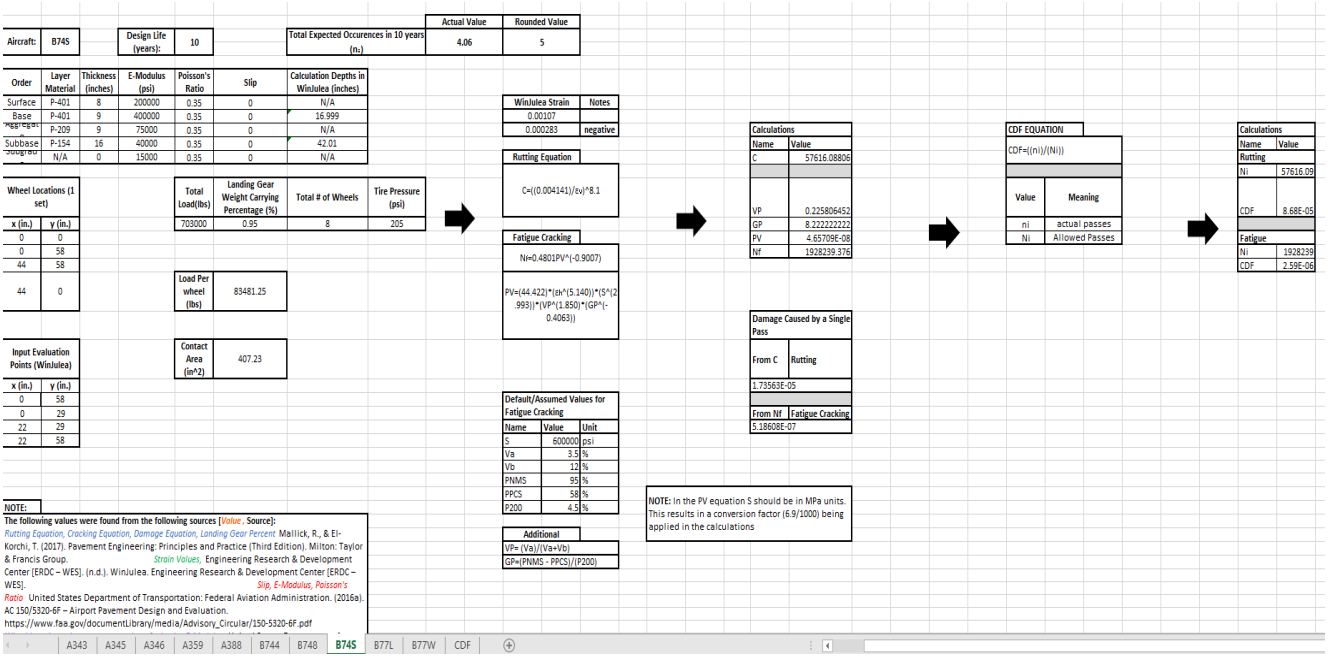

Aircraft:	B74S
Design Life (years):	10
Total Expected Occurences in 10 years (n_t)	Actual Value: 4.06 / Rounded Value: 5

Order	Layer Material	Thickness (inches)	E-Modulus (psi)	Poisson's Ratio	Slip	Calculation Depths in WinJulea (inches)
Surface	P-401	8	200000	0.35	0	N/A
Base	P-401	9	400000	0.35	0	16.999
Aggregate	P-209	9	75000	0.35	0	N/A
Subbase	P-154	16	40000	0.35	0	42.01
Subgrade	N/A	0	15000	0.35	0	N/A

Wheel Locations (1 set)	
x (in.)	y (in.)
0	0
0	58
44	58
44	0

Total Load(lbs)	Landing Gear Weight Carrying Percentage (%)	Total # of Wheels	Tire Pressure (psi)
703000	0.95	8	205

Load Per wheel (lbs)	83481.25
Contact Area (in^2)	407.23

Input Evaluation Points (WinJulea)	
x (in.)	y (in.)
0	58
0	29
22	29
22	58

WinJulea Strain	Notes
0.00107	
0.000283	negative

Rutting Equation

C=((0.004141)/εv)^8.1

Fatigue Cracking

Nf=0.4801PV^(-0.9007)

PV=(44.422)*(εt^(5.140))*(S^(2.993))*(VP^(1.850)*(GP^(-0.4063))

Default/Assumed Values for Fatigue Cracking		
Name	Value	Unit
S	600000	psi
Va	3.5	%
Vb	12	%
PNMS	95	%
PPCS	58	%
P200	4.5	%

Additional

VP= (Va)/(Va+Vb)

GP=(PNMS - PPCS)/(P200)

Calculations	
Name	Value
C	57616.08806
VP	0.225806452
GP	8.222222222
PV	4.65709E-08
Nf	1928239.376

Damage Caused by a Single Pass	
From C	Rutting
1.73563E-05	
From Nf	Fatigue Cracking
5.18608E-07	

NOTE: In the PV equation S should be in MPa units. This results in a conversion factor (6.9/1000) being applied in the calculations

CDF EQUATION	
CDF=((ni)/(Ni))	
Value	Meaning
ni	actual passes
Ni	Allowed Passes

Calculations	
Name	Value
Rutting	
Ni	57616.09
CDF	8.68E-05
Fatigue	
Ni	1928239
CDF	2.59E-06

NOTE:
The following values were found from the following sources [*Value* , **Source**]:
Rutting Equation, Cracking Equation, Damage Equation, Landing Gear Percent Mallick, R., & El-Korchi, T. (2017). Pavement Engineering: Principles and Practice (Third Edition). Milton: Taylor & Francis Group.
Strain Values, Engineering Research & Development Center [ERDC – WES]. (n.d.). WinJulea. Engineering Research & Development Center [ERDC – WES].
Slip, E-Modulus, Poisson's Ratio United States Department of Transportation: Federal Aviation Administration. (2016a). AC 150/5320-6F – Airport Pavement Design and Evaluation. https://www.faa.gov/documentLibrary/media/Advisory_Circular/150-5320-6F.pdf

A343 | A345 | A346 | A359 | A388 | B744 | B748 | B74S | B77L | B77W | CDF

Figure B-8: Design 1.2 Aircraft B74S

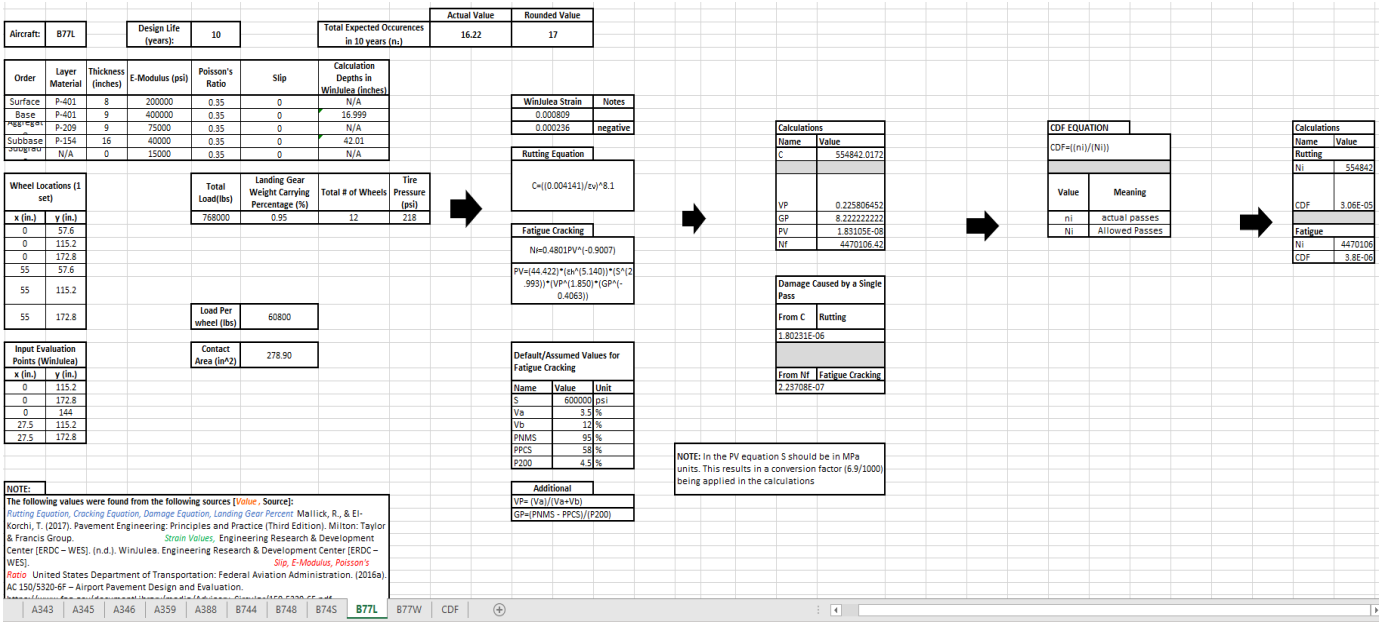

Aircraft:	B77L	Design Life (years):	10	Total Expected Occurences in 10 years (n_t)	Actual Value: 16.22	Rounded Value: 17

Order	Layer Material	Thickness (inches)	E-Modulus (psi)	Poisson's Ratio	Slip	Calculation Depths in WinJulea (inches)
Surface	P-401	8	200000	0.35	0	N/A
Base	P-401	9	400000	0.35	0	16.999
Aggregat.	P-209	9	75000	0.35	0	N/A
Subbase	P-154	16	40000	0.35	0	42.01
Subgrad.	N/A	0	15000	0.35	0	N/A

WinJulea Strain	Notes
0.000809	
0.000236	negative

Wheel Locations (1 set)	
x (in.)	y (in.)
0	57.6
0	115.2
0	172.8
55	57.6
55	115.2
55	172.8

Total Load(lbs)	Landing Gear Weight Carrying Percentage (%)	Total # of Wheels	Tire Pressure (psi)
768000	0.95	12	218

Load Per wheel (lbs)	60800
Contact Area (in^2)	278.90

Input Evaluation Points (WinJulea)	
x (in.)	y (in.)
0	115.2
0	172.8
0	144
27.5	115.2
27.5	172.8

Rutting Equation

$C=((0.004141)/\varepsilon_v)^{8.1}$

Fatigue Cracking

$N_f=0.4801PV^{(-0.9007)}$

$PV=((44.422)*(\varepsilon_t^{(5.140)})*(S^{(2.993)})*(VP^{(1.850)})*(GP^{(-0.4063)}))$

Default/Assumed Values for Fatigue Cracking		
Name	Value	Unit
S	600000	psi
Va	3.5	%
Vb	12	%
PNMS	95	%
PPCS	58	%
P200	4.5	%

Additional
VP= (Va)/(Va+Vb)
GP=(PNMS - PPCS)/(P200)

Calculations	
Name	Value
C	554842.0172
VP	0.225806452
GP	8.222222222
PV	1.83105E-08
Nf	4470106.42

Damage Caused by a Single Pass	
From C	Rutting
1.80231E-06	
From Nf	Fatigue Cracking
2.23708E-07	

NOTE: In the PV equation S should be in MPa units. This results in a conversion factor (6.9/1000) being applied in the calculations

CDF EQUATION
CDF=((ni)/(Ni))

Value	Meaning
ni	actual passes
Ni	Allowed Passes

Calculations	
Name	Value
Rutting	
Ni	554842
CDF	3.06E-05
Fatigue	
Ni	4470106
CDF	3.8E-06

NOTE:

The following values were found from the following sources [*Value*, Source]:

Rutting Equation, Cracking Equation, Damage Equation, Landing Gear Percent Mallick, R., & El-Korchi, T. (2017). Pavement Engineering: Principles and Practice (Third Edition). Milton: Taylor & Francis Group. *Strain Values,* Engineering Research & Development Center [ERDC – WES]. (n.d.). WinJulea. Engineering Research & Development Center [ERDC – WES]. *Slip, E-Modulus, Poisson's Ratio* United States Department of Transportation: Federal Aviation Administration. (2016a). AC 150/5320-6F – Airport Pavement Design and Evaluation.

A343 | A345 | A346 | A359 | A388 | B744 | B748 | B74S | B77L | B77W | CDF

Figure B-9: Design 1.2 Aircraft B77L

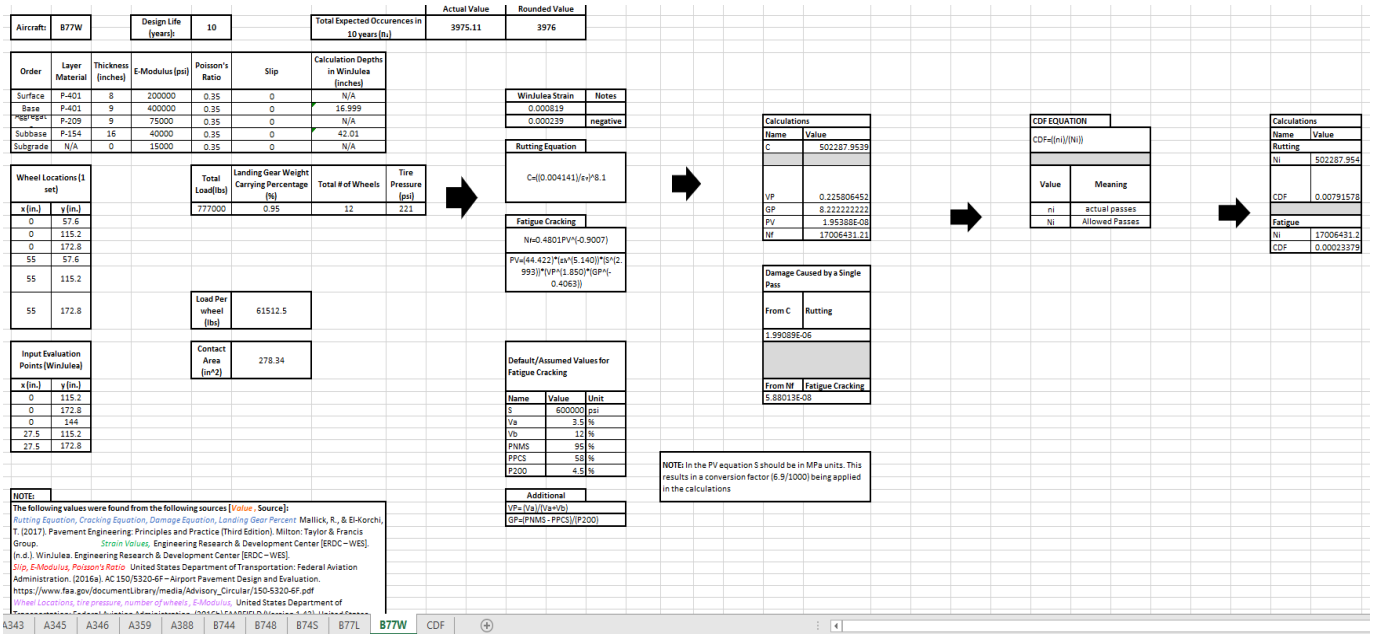

Aircraft:	B77W	Design Life (years):	10	Total Expected Occurences in 10 years (n_t)	Actual Value: 3975.11	Rounded Value: 3976

Order	Layer Material	Thickness (inches)	E-Modulus (psi)	Poisson's Ratio	Slip	Calculation Depths in WinJulea (inches)
Surface	P-401	8	200000	0.35	0	N/A
Base	P-401	9	400000	0.35	0	16.999
Aggregat.	P-209	9	75000	0.35	0	N/A
Subbase	P-154	16	40000	0.35	0	42.01
Subgrade	N/A	0	15000	0.35	0	N/A

WinJulea Strain	Notes
0.000819	
0.000239	negative

Wheel Locations (1 set)	
x (in.)	y (in.)
0	57.6
0	115.2
0	172.8
55	57.6
55	115.2
55	172.8

Total Load(lbs)	Landing Gear Weight Carrying Percentage (%)	Total # of Wheels	Tire Pressure (psi)
777000	0.95	12	221

Load Per wheel (lbs)	61512.5
Contact Area (in^2)	278.34

Input Evaluation Points (WinJulea)	
x (in.)	y (in.)
0	115.2
0	172.8
0	144
27.5	115.2
27.5	172.8

Rutting Equation

$C=((0.004141)/\varepsilon_v)^{8.1}$

Fatigue Cracking

$N_f=0.4801PV^{(-0.9007)}$

$PV=((44.422)*(\varepsilon_t^{(5.140)})*(S^{(2.993)})*(VP^{(1.850)})*(GP^{(-0.4063)}))$

Default/Assumed Values for Fatigue Cracking		
Name	Value	Unit
S	600000	psi
Va	3.5	%
Vb	12	%
PNMS	95	%
PPCS	58	%
P200	4.5	%

Additional
VP= (Va)/(Va+Vb)
GP=(PNMS - PPCS)/(P200)

Calculations	
Name	Value
C	502287.9539
VP	0.225806452
GP	8.222222222
PV	1.95388E-08
Nf	17006431.21

Damage Caused by a Single Pass	
From C	Rutting
1.99089E-06	
From Nf	Fatigue Cracking
5.88013E-08	

NOTE: In the PV equation S should be in MPa units. This results in a conversion factor (6.9/1000) being applied in the calculations

CDF EQUATION
CDF=((ni)/(Ni))

Value	Meaning
ni	actual passes
Ni	Allowed Passes

Calculations	
Name	Value
Rutting	
Ni	502287.954
CDF	0.00791578
Fatigue	
Ni	17006431.2
CDF	0.00023379

NOTE:

The following values were found from the following sources [*Value*, Source]:

Rutting Equation, Cracking Equation, Damage Equation, Landing Gear Percent Mallick, R., & El-Korchi, T. (2017). Pavement Engineering: Principles and Practice (Third Edition). Milton: Taylor & Francis Group. *Strain Values,* Engineering Research & Development Center [ERDC – WES]. (n.d.). WinJulea. Engineering Research & Development Center [ERDC – WES]. *Slip, E-Modulus, Poisson's Ratio* United States Department of Transportation: Federal Aviation Administration. (2016a). AC 150/5320-6F – Airport Pavement Design and Evaluation. https://www.faa.gov/documentLibrary/media/Advisory_Circular/150-5320-6F.pdf *Wheel Locations, tire pressure, number of wheels , E-Modulus,* United States Department of

A343 | A345 | A346 | A359 | A388 | B744 | B748 | B74S | B77L | B77W | CDF

Figure B-10: Design 1.2 Aircraft B77W

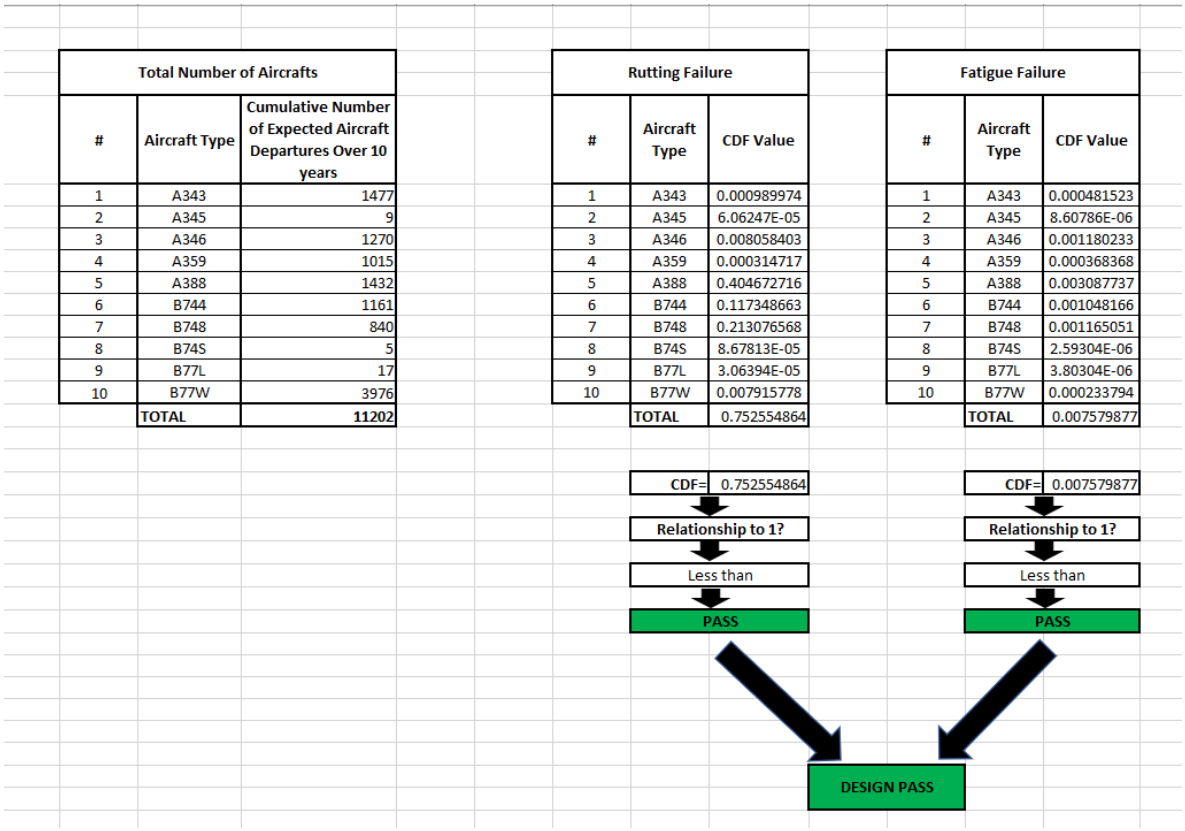

Total Number of Aircrafts		
#	Aircraft Type	Cumulative Number of Expected Aircraft Departures Over 10 years
1	A343	1477
2	A345	9
3	A346	1270
4	A359	1015
5	A388	1432
6	B744	1161
7	B748	840
8	B74S	5
9	B77L	17
10	B77W	3976
	TOTAL	11202

Rutting Failure		
#	Aircraft Type	CDF Value
1	A343	0.000989974
2	A345	6.06247E-05
3	A346	0.008058403
4	A359	0.000314717
5	A388	0.404672716
6	B744	0.117348663
7	B748	0.213076568
8	B74S	8.67813E-05
9	B77L	3.06394E-05
10	B77W	0.007915778
	TOTAL	0.752554864

Fatigue Failure		
#	Aircraft Type	CDF Value
1	A343	0.000481523
2	A345	8.60786E-06
3	A346	0.001180233
4	A359	0.000368368
5	A388	0.003087737
6	B744	0.001048166
7	B748	0.001165051
8	B74S	2.59304E-06
9	B77L	3.80304E-06
10	B77W	0.000233794
	TOTAL	0.007579877

Figure B-11: Design 1.2 Cumulative Damage Factors